Pou5f3 and Sox19b select gene expression repertoire at Zygotic Genome Activation

Meijiang Gao*[,1], Marina Veil*[,1], Marcus Rosenblatt[2], Anna Gebhard[1], Helge Hass[2], Lenka Buryanova[1], Lev Y. Yampolsky[3,4], Björn Grüning[5,6], Jens Timmer[2,7], Daria Onichtchouk**[1,7,8]

***contributed equally**

[1]Department of Developmental Biology, Albert-Ludwigs-University of Freiburg, 79104 Freiburg, Germany

[2]Institute of Physics, Albert-Ludwigs-University of Freiburg, 79104 Freiburg, Germany

[3]Department of Biological Sciences, East Tennessee State University, Johnson City, Tennessee 37614-1710, USA

[4]Zoological Institute, Basel University, Basel CH-4051, Switzerland

[5]Department of Computer Science, Albert-Ludwigs-University of Freiburg, 79110 Freiburg, Germany

[6]Center for Biological Systems Analysis (ZBSA), Albert-Ludwigs-University of Freiburg, 79110 Freiburg, Germany

[7]Signalling Research centers BIOSS and CIBSS, 79104 Freiburg, Germany

[8]Institute of Developmental Biology RAS, 119991 Moscow, Russia

**Correspondence to: daria.onichtchouk@biologie.uni-freiburg.de

Abstract

PouV and SoxB1 family transcription factors (TFs) have emerged as master regulators of cell fate transitions. To investigate the genetic interactions between Pou5f3 and Sox19b in zebrafish embryos passing through Zygotic Genome Activation (ZGA), we combined time-resolved mutant transcription analysis using the novel tool RNA-sense, chromatin state and phenotypic assays. We distinguish four types of embryonic enhancers, differentially regulated by the two TFs. Pou5f3 is critical for activation of enhancer types 1 and 2, which are responsible for transcription of genes involved in gastrulation and ventral genes. Pou5f3 or Sox19b prevent premature activation of type 3 and 4 enhancers, which are responsible for transcription of organogenesis regulators, differentiation factors and dorsal genes. We also show that the balance between Sox19b and Pou5f3 is important for bulk ZGA timing. Our results uncover how independent activities of maternal Pou5f3 and Sox19b add up or antagonize to determine the early gene expression repertoire.

Bullet points:

- **Pou5f3 and Sox19b bind independently to DNA**
- **Disbalance between maternal Pou5f3 and Sox19b delays ZGA**
- **Pou5f3 suppresses premature transcription of neural patterning genes, activated by SoxB1 factors**
- **Pou5f3 and Sox19b synergistically suppress premature transcription of a wide range of differentiation genes**
- **Pou5f3 and Sox19b restrict the dorsal organizer**

Introduction

Following fertilization, the differentiated cells, egg and sperm, are reprogrammed into the totipotent state of the resulting zygote. The zygotic genome remains initially silent, while reprogramming takes place. The zygotic genome awakens through a process known as maternal-to-zygotic transition (MZT), during which the degradation of maternal transcripts is coordinated with Zygotic Genome Activation (ZGA). The current models of ZGA take into account the gradual increase in the ratio of transcriptional activators to transcriptional repressors, accompanied with local changes of chromatin accessibility, which together create a permissive environment for ZGA to occur (Schulz and Harrison, 2018; Vastenhouw et al., 2019). In zebrafish, *Xenopus* and *Drosophila*, where development starts with rapid cell cycles, excessive maternal core histones serve as general transcriptional repressors before ZGA occurs (Almouzni and Wolffe, 1995; Amodeo et al., 2015; Joseph et al., 2017; Shindo and Amodeo, 2019; Wilky et al., 2019). Activators that are translated before ZGA and reach critical levels at ZGA include three types of proteins: basal transcription factors (Ferg et al., 2007; Veenstra et al., 1999), the regulators of H3K27ac enhancer mark (Chan et al., 2019; Sato et al., 2019) and maternal transcription factors (TFs). TFs that broadly activate zygotically expressed genes have been identified in *Drosophila* (Zelda, Liang et al., 2008), zebrafish (Pou5f3, Sox19b and Nanog, Lee et al., 2013; Leichsenring et al., 2013), *Xenopus* (Pou5f3 and Sox3, Gentsch et al., 2019), human (POU5F1, DUX4, Gao et al., 2018; Hendrickson et al., 2017), and mouse (Nfya, Dux, Dppa2 and Dppa4, De Iaco et al., 2017; Eckersley-Maslin et al., 2019; Lu et al., 2016).

Nucleosome positioning plays a dominant role in regulating DNA access by TFs (He et al., 2010; Klemm et al., 2019). The widespread action of sequence-specific TFs during ZGA is thought to reside on their ability to act as pioneer factors, first displacing nucleosomes, so that other TFs can also bind (Iwafuchi-Doi and Zaret, 2016; McDaniel et al., 2019; Schulz et al., 2015; Sun et al., 2015; Veil et al.,2019; Palfy et al., 2020). In case of several TFs, like in zebrafish, it remains an open question, how they divide the labor of activating the zygotic genome, as well as the question how their broad pioneer activity at ZGA relates to their different functions during gastrulation, as inferred from mutant phenotypes (Gagnon et al., 2018; Lunde et al., 2004; Okuda et al., 2010; Veil et al., 2019). In zebrafish embryos, a block of maternal and zygotic Pou5f3 function leads to epiboly defects and developmental arrest during gastrulation, while the block of all early expressed redundant SoxB1 family members (Sox19a, Sox19b, Sox3 and Sox2) leads to developmental arrest at the beginning of organogenesis.

Mammalian homologs of zebrafish genome activators, Pou5f1 and Sox2, are the major components of transcription factor cocktails used for reprogramming of somatic cells to pluripotency (Takahashi and Yamanaka, 2006), and are proven sufficient for reprogramming in several documented cases (Giorgetti et al., 2010; Huangfu et al., 2008; Montserrat et al., 2012). The mechanisms underlying their partnership *in-vivo* are still not resolved. Until recently, Pou5f1 and Sox2 were thought to act cooperatively, binding as heterodimers to bipartite *pou:sox* cognate motifs (Boyer et al., 2005; Loh et al., 2006; Remenyi et al., 2003). This dominating view was challenged by Soufi et al., (2015), who demonstrated that Pou5f1 and Sox2 bind different motifs on the nucleosome-wrapped DNA, and by four recent studies in ES cells which suggested four different scenarios of how Pou5f1 and Sox2 interact with each other and with chromatin. These scenarios are: 1) assisted loading (Chen et al., 2014); 2) negative reciprocity: Pou5f1 and Sox2 sometimes help and sometimes hinder each other in binding across the genome (Biddle et al., 2019); 3) conditional cooperativity: depending on the motif positions in the nucleosomal context (Li et al., 2019); and 4) independent binding (Friman et al., 2019). The embryonic phenotypes of mouse Pou5f1 and Sox2 mutants are different, suggesting unique biological roles of each TF (Avilion et al., 2003; Frum et al., 2013; Wicklow et al., 2014; Wu et al., 2013).

Before the terms MZT and ZGA were coined (Gerhart, 1980; Newport and Kirschner, 1982a, b; Signoret and Lefresne, 1971), Alexander Neyfakh performed a series of experiments inactivating nuclear function in teleost fish embryos by X-ray irradiation. Neyfakh's experiments revealed two distinct periods of zygotic gene expression which he called "morphogenetic nuclear function". The first period spanned from mid to late blastula and provided the instructions for whole gastrulation. The second period started at midgastrula and provided the instructions for differentiation and patterning of the tissues during organogenesis (Neyfakh, 1959, 1964). "Morphogenetic nuclear function" reflects the first and second waves of zygotic transcription, as was shown shortly afterwards (Bachvarova et al., 1966; Kafiani et al., 1969). From the standpoint of Neyfakh's concept, Pou5f3 function is critical for the first zygotic period, and SoxB1 for the second, in particular within the neural system. The earlier function for SoxB1 proteins was suggested by dominant-negative approaches (Shih et al., 2010; Zhang and Klymkowsky, 2007), and by combined morpholino knockdowns of SoxB1 with Nanog and/or Pou5f3 (Lee et al., 2013). However, the mechanisms of early SoxB1 activity and its molecular connection to Pou5f3 were not characterized.

Here, we investigate epistatic relationships between Pou5f3 and Sox19b, the only maternally expressed member of the SoxB1 family. We show that the two factors bind independently to DNA. Further, we demonstrate that Sox19b assists Pou5f3 loading onto a subset of enhancers of the first zygotic period genes which are directly activated by Pou5f3. Unexpectedly, simultaneous ablation of Pou5f3 and Sox19b does not result in ZGA delay, but leads to a burst of premature expression of the second period genes which normally regulate tissue differentiation at organogenesis stages.

Results

Genetic ablation of maternal Sox19b delays embryo development from ZGA till the end of gastrulation.

To abolish the expression of maternal SoxB1 in zebrafish, we introduced a mutation in *sox19b* by using the TALEN technique (Cermak et al., 2011). We chose an 8 bp deletion after the codon for amino acid 11 which resulted in introduction of a premature stop codon after another 62 amino acids (Fig. 1A). The zygotic mutants were indistinguishable from control (data not shown). To produce MZ*sox19b* embryos lacking both maternal and zygotic Sox19b, we crossed the mutant females with the mutant males. Such MZ*sox19b* mutants developed into viable and fertile adults, although the embryos tended to be smaller in size than wild-type. Significantly, however, the MZ*sox19b* mutants developed slower than controls (Movie S1-1).

Zebrafish embryos are first going through 9 rapid synchronous cell cycles and a longer meta-synchronous 10th cell cycle, followed by ZGA at 3 hours post-fertilization (hpf) (Kane and Kimmel, 1993; Keller et al., 2008). To determine the earliest time point of developmental delay, we visualized the nuclei in living wild-type and MZ*sox19b* mutant embryos by SYTOX green microinjection, video-recorded the embryos starting at 64 cell stage, and then compared the duration of pre-ZGA cell cycles between these genotypes. We did not detect statistically significant differences in the cycles 6-9 (Fig. S1A). To compare the duration of 10th cell cycle, we fixed WT and MZ*sox19b* embryos every 15 min starting from 2.5 hpf till 4 hpf, and compared the size of the cells and number of nuclei between the genotypes. We could detect that the MZ*sox19b* were still at the 512 cell stage (10th cell cycle), while the WT embryos proceeded to the 1024 cell stage (Fig.1B). Within the next 15 min MZ*sox19b* also completed 10th cell cycle. The time gap between MZ*sox19b* and wild-type increased up to one hour at 6 hpf, and up to two hours at 10 hpf (*i.e*. at the end of gastrulation). No further delay occurred during organogenesis (Fig. 1C and accompanying legend, summarized in Fig.1D).

Developmental delay was reflected in the molecular patterning of the MZ*sox19b* mutants. Subdivision of the ectoderm into neural and non-neural parts occurs at midgastrulation (8 hpf), and is accompanied by restriction of zygotic SoxB1 family members *sox19a, sox3 and sox2* to neuroectoderm (Dee et al., 2007; Okuda et al., 2006). Neuroectoderm formation was delayed in MZ*sox19b*, as ubiquitous SoxB1 distribution persisted until 8 hpf (Fig.2B, Fig. S1B). To summarize, we conclude that maternal Sox19b is involved in setting the speed of early developmental events starting from ZGA up to the end of gastrulation.

Developmental timing is sensitive to the maternal Sox19b/Pou5f3 balance

Normal development of MZ*sox19b* embryos is plausibly explained by the presence of functionally redundant SoxB1 family members, expressed shortly after ZGA: Sox2, Sox3 and Sox19a (Fig.2B). Direct transcriptional targets of SoxB1 regulation, *her3* and *hesx1* (Okuda et al., 2006; Onichtchouk et al., 2010), are expressed in MZ*sox19b* at 8 hpf indicating zygotic SoxB1 activity (Fig. S1C). Quadruple SoxB1 morpholino knockdown of Sox19b, Sox19a, Sox2 and Sox3 (SoxB1 QKD: Okuda et al., 2010) resulted in severe defects in tailbud formation, anterior-posterior axis elongation and neural system development. The earlier functions of SoxB1 genes could be masked by maternal Sox19b protein, detectable in SoxB1 QKD (Leichsenring et al., 2013). We completely removed SoxB1 activity by injecting Sox3, Sox19a and Sox2 morpholinos

into MZ*sox19b* mutant embryos (a triple-knockdown, or TKD) to address if SoxB1 genes functionally contribute to development from early to midgastrulation. MZ*sox19b*-TKD and WT- QKD showed similar defects (Fig. 2B), which could be rescued by co-injection of *sox19b* mRNA (Fig. S1D). We concluded that maternal and zygotic functions of SoxB1 proteins are uncoupled: zygotic SoxB1 activity becomes critical starting from the end of gastrulation, maternal Sox19b protein sets the timing of gastrulation (see Fig. 2F, H).

To take into account the interactions of maternal Sox19b with Pou5f3, we obtained a double mutant by crossing MZ*sox19b* to Pou5f3 mutant MZ*spg* ^{m793} (Lunde et al., 2004). MZ*spg* mutants develop severe epiboly defects which lead to gastrulation arrest (Eckerle et al., 2018; Song et al., 2013) and are weakly dorsalized (Belting et al., 2011; Reim and Brand, 2006). Epiboly defects in double MZ*sox19bspg* mutants were similar to MZ*spg* (Fig. 2C, Fig. S1E), but dorsalization was stronger (Fig.S1F). Surprisingly, the double mutants were less delayed than the single mutants, with the order of developmental delay MZ*sox19b*>MZ*spg*>MZ*sox19bspg* (Movie S1-2, 3). We produced maternal-only M*sox19bspg* mutants by fertilizing the mutant eggs with wild-type sperm, to find out if a combined maternal contribution of Pou5f3 and Sox19b is critical for developmental timing, epiboly, or dorso-ventral (D/V) patterning. Single mutants M*sox19b* and M*spg* developed without abnormalities but were developmentally delayed compared to the wild-type (M*sox19b*>M*spg*>M*sox19bspg*=WT). The double mutants were not delayed, but became severely dorsalized (Fig. 2D, E, Movie S1-4, 5). The observation, that maternal Sox19b and Pou5f3 compensated each other's effects on developmental timing, suggested that they were acting antagonistically (Fig. 2F). The observation, that the double, but not the single mutants are overtly dorsalized, suggested that at least one maternal TF, Pou5f3 or Sox19b should be present to safeguard normal dorso-ventral patterning of the embryo (Fig. 2G). Finally, Pou5f3 was required for epiboly, while SoxB1 was dispensable (Fig. 2H). To understand the molecular nature of Pou5f3 and Sox19b interactions, we examined the changes in chromatin accessibility, histone modifications and transcription in the mutants.

Sox19b and Pou5f3 act as independent pioneer factors and displace nucleosomes on high nucleosome affinity regions (HNARs) using different binding cues.

Loss of the maternal transcription factors Pou5f3, Sox19b, and Nanog results in decreased accessibility at regulatory elements (Liu et al., 2018; Palfy et al., 2020). We have recently shown that shortly after ZGA Pou5f3, SoxB1 and Nanog recognize their consensus motifs in the context of the High Nucleosome Affinity Regions (HNARs). 600 bp long HNARs are featuring high predicted *in-vitro* nucleosome occupancy and DNA shape parameter Propeller Twist (PT°) values. They are centered on a 300 bp rotational periodicity frame, which supports nucleosome positioning on one side of the DNA molecule. Pou5f3 and Nanog sequence-specifically displace nucleosomes on HNARs, bound by all three genome activators (PSN regions). In addition, at 4.3 hpf, Nanog non-consensus binding elicits a genome-wide nucleosome displacement effect, directly proportional to predicted *in-vitro* nucleosome occupancy values of HNARs (Veil et al., 2019).

To compare nucleosome displacement by Pou5f3 and Sox19b, we performed MNase-seq experiment on 4.3 hpf MZ*sox19b* mutants (STAR Methods). We ranked PSN regions by descending chromatin accessibility in the wild-type (Fig.3A), took HNAR centers as summits (Fig.3B) and plotted MNase signals in three genotypes (Fig.3C).

Nucleosome displacement by each factor was calculated as MNase signal difference between each mutant and wild-type (Fig.3D, Fig.S1G). We found that Pou5f3 displaced nucleosomes from the most accessible, “open” regions, while Sox19b affected both “open” and relatively “closed” regions within the central 300 bp of HNARs (Fig. 3CD, Fig. S1G). This observation suggested that Sox19b is able to engage into closed chromatin more efficiently than Pou5f3, perhaps by using different DNA recognition cues.

Next we asked which motifs contribute to nucleosome displacement by each TF. SoxB1 proteins can recognize two types of consensus sequences: bipartite HMG/POU *pou:sox* motifs and *sox* motifs (Fig. 3E; Hou et al., 2017), in the context of HNARs (Fig.3F; Veil et al., 2019). The density of *pou:sox,* but not *sox* motifs was higher in “open” chromatin regions (Fig. S1H). We assumed that, if the effects of TF were sequence-specific, the strength of the nucleosome displacement would increase with the number of cognate motifs per genomic region occupied by TF. We calculated the differences in MNase signals between the wild-type and each mutant (Δmut), on each PSN region (set as 320 bp, the mean size of TF ChIP-seq peak). We then compared the mean Δmut values for the PSN regions with no motifs, one motif, two motifs, three or more motifs of each type. We found that nucleosome displacement by Sox19b strongly increases with the number of *sox* motifs (and much weaker with *pou:sox* motifs) per region; Pou5f3 displaced nucleosomes only on *pou:sox* motifs (Fig. 3G, and Table S1 for statistics).

TFs preferentially occupy DNA with specific structures ("shape motifs") regardless of whether or not these correspond to high information content sequence motifs; the phenomenon called non-consensus binding (Aftek et al., 2015). When shape and sequence motifs co-occur, they can be overlapping, flanking, or separated by consistent spacing (Samee et al., 2019). The values of DNA shape parameter Propeller Twist (PT°) strongly correlate with *in-vitro* nucleosome prediction (Kaplan et al., 2009) within HNARs (Veil et al., 2019, Fig. 3F). SoxB1-bound genomic regions had in average higher *in-vitro* nucleosome prediction, than Pou5f3-bound (Fig. S1I), suggesting that these TFs may occupy different shape motifs. To infer non-consensus binding effects of Sox19b and Pou5f3, we compared the mean Δmut values for the regions with ascending *in-vitro* predicted nucleosome occupancy. We found that nucleosome displacement by Sox19b non-consensus binding was directly proportional to *in-vitro* predicted nucleosome occupancy, both on PSN regions and genome-wide. Nucleosome displacement by Pou5f3 showed the opposite tendency (Fig. 3H, Fig. S2A-G, Table S1 for statistics).

In sum, we demonstrate that Sox19b and Pou5f3 act as independent pioneer factors shortly after ZGA. They displace nucleosomes by binding to different consensus motifs on PSN regions. Non-consensus binding of two factors results in the opposing effects of local chromatin accessibility genome-wide.

Changes of the histone mark H3K27ac in MZ*sox19b* and MZ*spg* mutants define four types of differentially regulated embryonic enhancers.

In parallel with the increase of chromatin accessibility during ZGA, zebrafish genome acquires H3K27ac and H3K4me3 histone tail modification marks which correlate with active enhancers and promoters, respectively (Bogdanovic et al., 2012; Creyghton et al., 2010; Heintzman et al., 2007). Deposition of H3K27ac on early enhancers is functionally important for ZGA (Chan et al., 2019). To test if histone mark deposition

on genome regulatory elements depends on Pou5f3 and Sox19b, we immunoprecipitated embryonic chromatin originating from late blastula stage (dome, 4.3 hpf) of the WT, MZ*spg* and MZ*sox19b* embryos with H3K27ac and H3K4me3 antibodies, sequenced and compared the mapped data.

To infer the genome-wide enhancer activity changes in the mutants, we identified H3K27ac and H3K4me3 peaks in each genotype, removed H3K27ac peaks overlapping with H3K4me3 (promoters), and then clustered the list of unique peaks by H3K27ac signal in the three genotypes (STAR Methods, Table S2). This resulted in five clusters of H3K27ac peaks: 1) Pou5f3-activated, 2) Pou5f3 and Sox19b –activated, 3) Pou5f3-repressed, 4) Sox19b-repressed and 5) independent on Pou5f3 and Sox19b (Fig. 4A, Fig. S3A). H3K27ac peaks of clusters 1, 2, 4 and 5 associated with genes expressed during gastrulation, while cluster 3 associated with neural patterning genes expressed during organogenesis in GREAT analysis (Hiller et al., 2013; icons in Fig. 4A, Table S2). H3K27ac peaks of all clusters were surrounded by accessible chromatin enriched in Pou5f3, SoxB1, Nanog, Eomesodermin and FoxH1 binding (Fig. S3B,C); the last two maternal TFs are implicated in mesendoderm specification (Bruce et al., 2003; Du et al., 2012; Slagle et al., 2011). We concluded, that H3K27ac peaks mark genomic enhancers. Intriguingly, plotting the average *in-vitro* nucleosome prediction values around each of the five H3K27ac peak clusters resulted in five distinct profiles (Fig.S3D). This may reflect the differences in DNA shape underlying five enhancer types.

In sum, our results revealed genome-wide redistribution of H3K27ac mark in MZ*spg* and MZ*sox19b* mutants and allowed us to delineate five enhancer types. We further focused on differential enhancers, where H3K27 acetylation depended on Pou5f3 or Sox19b (types 1, 2, 3 and 4).

Pou5f3 binding, independent on Sox19b binding on type 1 enhancers, or assisted by Sox19b on type 2 enhancers, induces local H3K27 acetylation.
To distinguish between direct and indirect effects of Pou5f3 and Sox19b pioneer activity on H3K27ac, we accessed if the nucleosome displacement by Pou5f3 and Sox19b on their known binding sites coincides with the local H3K27ac gains or losses in the respective mutants. We selected PSN binding regions within +/- 500 bp from H3K27ac peaks and took HNAR centers as summits. We compared the H3K27ac occupancy in three genotypes with the nucleosome displacement by Pou5f3 and Sox19b, and the density of *sox* and *pou:sox* motifs for each enhancer type (Fig. 4B, Fig. S3E, F). Nucleosome displacement by Pou5f3 on *pou:sox* motifs was detectable on Pou5f3-activated (type 1) and Pou5f3 and Sox19b-activated (type 2) enhancers, which were also enriched in *pou:sox* motifs (Fig. 4B). Hence, Pou5f3 binding to type 1 and 2 enhancers directly induced nucleosome displacement and H3K27 acetylation of flanking nucleosomes.

Sox19b and Pou5f3 can act together or sequentially on type 2 enhancers. In the first scenario, Sox19b and Pou5f3 co-bind *pou:sox* motifs. In the second scenario, known as assisted loading (Voss et al., 2011), Sox19b destabilizes nucleosomes by binding to *sox* motifs, facilitating an access of Pou5f3 to *pou:sox* motifs nearby. To distinguish between the scenarios, we estimated if the binding of Sox19b to one of the motifs may be causal for H3K27 acetylation loss in MZ*sox19b* and *MZspg*. We calculated the differences in H3K27ac signals between the wild-type and each mutant (ΔH3K27ac), around each PSN region (+/- 500bp from max). Comparing the mean ΔH3K27ac

values for the regions with no motifs, one motif, two motifs or three or more, we found that local H3K27ac deposition depends only on Sox19b binding to *sox* motifs, or only on Pou5f3 binding to *pou:sox* motifs (Fig.4C, Table S1 for statistics). The most parsimonious explanation of the results is that Sox19b binding to *sox* motifs facilitates an access to chromatin for Pou5f3. Pou5f3 acts downstream of Sox19b, binds to *pou:sox* motifs within the same HNAR, and induces local H3K27 acetylation.

As a rule, independent (type 5) and differential (types 1-4) enhancers were intermingled in the proximity of developmental genes (Table S2), suggesting complex combinatorial regulation. Only in a handful of cases, H3K27ac was gained or lost over 5-50 kb around the genes according to one pattern. To get clear regulatory examples, we picked 7-13 "top genes" for each differential enhancer type (Fig.4 D-G and Fig. S4A-D). The top type 1 genes included direct transcriptional targets of Pou5f3: *klf17* (Fig.4D), *mych* and *klf2b* (Fig.S4A; Kotkamp et al., 2014a; Kotkamp et al., 2014b). In MZ*sox19b* H3K27ac around top type 1 genes was unchanged or gained (*foxi, klf2b* and *cyp24a1,* Fig. S4A). Around top type 2 genes, H3K27ac was lost in both mutants (Fig. 4E, Fig. S4B). We concluded, that on type 1 enhancers Sox19b binding was dispensable for H3K27ac or prevented it. On type 2 enhancers, Sox19b assisted Pou5f3 loading.

Enhancers repressed by Pou5f3 (type 3) are often located near SoxB1 target genes, and enhancers repressed by Sox19b (type 4) near Eomesodermin/FoxH1 target genes

Repression of H3K27ac by Pou5f3 (on type 3 enhancers), or by Sox19b (on type 4 enhancers) occurred without nucleosome displacement by respective TFs (Fig.4B). However, Sox19b displaced nucleosomes on type 3 enhancers (Fig.4B). Type 3 enhancers were enriched in *sox* motifs and associated with late neural genes (Fig.4AB, Table S2), suggesting that some of them are SoxB1 – activated. Indeed, 7/13 top cluster 3 genes were known SoxB1 targets (*pcdh18b, tp63, pdgfaa, msx3, rx3, nr2f5* and *lhx5;* Okuda et al., 2010). Most of type 3 enhancers were inactive in the 4.3 hpf wild-type embryos, in agreement with the late expression of nearby genes (Fig.4F, Fig.S4C, Okuda et al., Ruzicka et al., 2019). When H3K27ac was present in the wild-type, it was lost in MZ*sox19b* but gained in MZ*spg* (*pcdh18b* at Fig. 4F, *tp63* in Fig. S4C). Taken together, the data suggested that Pou5f3 prevented premature activation of type 3 enhancers by SoxB1 binding. Since no pioneer activity of Pou5f3 was detectable, we assumed that Pou5f3 may repress type 3 enhancers indirectly.

Type 4 enhancers were not enriched in *sox* or *pou:sox* motifs, neither Sox19b nor Pou5f3 displaced nucleosomes (Fig.4B, Fig.S3F). In spite of that, chromatin on type 4 enhancers was accessible (Fig. S3G). As Eomesodermin, FoxH1 and Nanog ChIP-seq signals colocalized with HNAR centers (Fig.S3H), we assumed that these factors may activate type 4 enhancers. Indeed, 4/7 of top type 4 genes were Eomesodermin/FoxH1 targets: *noggin1, chordin, noto* and *fscn1a* (Shimizu et al., 2000; Sirotkin et al., 2000; Fekany et al., 1999; Talbot et al., 1995; Liu et al., 2016). Around top type 4 genes, the H3K27ac mark was gained not only in MZ*sox19b* but also in MZ*spg*, in somewhat different genomic locations (Fig. S4D).

H3K27ac changes in the mutants are predictive for transcriptional changes.

Using selected "top genes", we addressed the question, if H3K27ac changes at four differential enhancer types are predictive for the transcriptional outcome in the mutants. To compare the single and double mutant effects on gene expression, we

performed RNA-seq time-series analysis using the wild-type (w), MZ*sox19b* (s), MZ*spg* (p) and double (d) mutants. The embryos were collected every 30 minutes starting from 2.5 hpf (pre-ZGA) till 6 hpf (midgastrula, Fig.5A).

Transcription of top genes driven by Pou5f3-activated (type 1) enhancers was identically repressed in MZ*spg* and double mutant over time, while in MZ*sox19b* the transcriptional profiles were different (Fig. 5B, Fig. S5A). For example, transcription of *klf2b*, *foxi* and *cyp24a1* was completely lost in and MZ*spg* and MZ*sox19bspg*, but increased in MZ*sox19b* over WT (Fig. S5A). This suggested that all Sox19b effects on H3K27 acetylation and transcriptional activation by type 1 enhancers were mediated via Pou5f3. Transcription driven by Pou5f3- and Sox19b –activated (type 2) enhancers initiated only in the wild-type, but not in the mutants (Fig. 5B, Fig. S5B), in agreement with the model of Pou5f3 assisted loading on type 2 enhancers.

Transcription driven by Pou5f3-repressed (type 3) enhancers was low within our time frame. 5/13 genes were transcriptionally active in the wild-type and repressed in MZ*sox19b* (*pcdh18* in Fig.5B; *tp63, msx3*, *lhx5*, *il34*, Fig. S5C), supporting proposed activation by SoxB1 TFs. 12/13 of top type 3 genes were overactivated in MZ*spg,* and 10/13 in double mutants, with somewhat slower dynamics (Fig.5B, Fig. S5C). Transcription of genes driven by Sox19b-repressed (type 4) enhancers was overactivated in the double mutant (7/8 genes, *noggin1* in Fig 5B; *fscn1a*, *frem1b*, *cdc25b*, *noto*, *cited4a*, *cldnb* in Fig. S5D).

In sum, the activation or repression of H3K27ac mark on four differential enhancer types in Pou5f3 and Sox19b mutants were predictive for transcriptional changes for the selected genes. Our next step was to extend time-resolved mutant transcriptional analysis to the whole genome.

RNA-seq time resolved analysis reveals that bulk transcriptional timing at ZGA is sensitive to the Sox19b/Pou5f3 balance.

Two processes shape the transcriptional landscape of embryos at ZGA: the burst of zygotic transcription and regulated decay of maternal mRNAs. About 70% of zebrafish mRNAs are maternally loaded (Harvey et al., 2013), so that the mRNA present in the embryo at each given early time point is a mix of maternal and zygotic transcripts for most genes. To account for the maternal and zygotic differences between the wild-type and mutants, we developed a novel tool for dynamic RNA-seq data analysis, which we called RNA-sense (the principle is described below, see Fig.S6 AB and STAR Methods for the details).

The RNA-sense tool compares RNA-seq time curves in two experimental conditions, *i.e*. the wild-type and mutant, and works in three steps. At Step 1, it builds a time profile for each transcript in one condition (*i.e.* wild-type) and tests if the transcript abundance grows or decays significantly. Dynamic transcripts are then sorted to non-overlapping groups by the time point of switch up (mostly zygotic transcripts, Fig.S6A), or switch down (mostly maternal transcripts, Fig.S6B). At Step 2, RNA-sense outputs the groups of differentially expressed transcripts, which are up- or downregulated in the mutant compared to the wild-type, for each time point. Correlations between the outputs of Step 1 and Step 2 are calculated at Step 3. The results of the correlation analysis are printed as two-dimensional color plot, with time profiles and differential expression groups at Y- and X-axis, which facilitates the interpretation of the data.

In general, “switch up” and “switch down” time profile groups generated by RNA-sense matched to zygotic and maternal transcripts identified in three studies (Fig. S6 C, Table S3; Haberle et al., 2014; Harvey et al., 2013; Lee et al., 2013), and will be referred as “zygotic” and “maternal” genes below.

RNA-sense analysis using the wild-type dynamic time profiles (4.605 zygotic and 3.584 maternal transcripts, Table S3) revealed delays in zygotic transcription and maternal mRNA degradation in all mutants (Fig.5C, Fig.S6 D). We compared the scope of ZGA delays in single and double mutants by scoring the number of wild-type zygotic transcripts, downregulated in at least one point at or after the switch up (to the right from the white line in Fig.5C). Out of three genotypes, the number of downregulated zygotic genes was the largest in MZ*sox19b* (63%), intermediate in MZ*spg* (34%) and the smallest in the double mutant MZ*sox19bspg* (25%, Fig 5D). We next compared the scope of maternal mRNA degradation in the mutants, by scoring the maternal transcripts upregulated in at least one time point after the switch down. Again, the number of upregulated maternal genes was the highest in MZ*sox19b* (58%), intermediate in MZ*spg* (29%) and the smallest in the double mutants (19%, Fig. S6E). The same order of change (MZ*sox19b* >MZ*spg*>MZ*sox19bspg*) was evident when comparing the mean expression (from 2.5 to 6 hpf) for maternal and zygotic transcripts (Fig.S6F). Thus, the depletion of single TFs resulted in a stronger transcriptional delay than simultaneous depletion of both TFs. This indicated the genetic compensation of Pou5f3 and Sox19b in regard to the bulk ZGA. Unexpectedly, Pou5f3/Sox19b balance appeared to be more important for timely onset of bulk transcription, than the presence of both factors in the embryo.

Pou5f3 and Sox19b are dispensable for the zygotic activation of maternal ß-catenin and Eomesodermin/FoxH1 target genes.

To distinguish between general and specific delays of zygotic gene activation, we grouped the zygotic genes downregulated only in the single mutants, or in the double mutants (Fig. 5D, Fig. S7A), and scored the proportions of differential enhancers on their putative regulatory regions. The proportion of Pou5f3- activated enhancers (types 1 and 2) was above genomic average only for the genes downregulated in the double mutants (Fig.S7B), suggesting that Pou5f3, with or without Sox19b assistance, specifically activates only these genes.

9% of all zygotic genes were repressed in both single, but not in the double mutants (red frame in Fig. 5D, Fig.5E, Fig. S7C). Strikingly, this group included the earliest target of dorsal maternal ß-catenin *dharma/bozozok* (Leung et al., 2003), its direct targets *hhex* (Bischof and Driever, 2004), and *chordin* (Shimizu et al., 2000), and the critical components of the endomesoderm specification network, activated by Eomesodermin/FoxH1 and Nodal signaling: *mixl* (Kikuchi et al., 2000), *foxa3* (Dal-Pra et al., 2011), *sebox* (Poulain and Lepage, 2002), *sox32* (Kikuchi et al., 2001), *dusp4* (Brown et al., 2008), *noto* (Talbot et al., 1995) and *tbxta* (Schulte-Merker et al., 1994) (see Fig. 5E, Fig.S7A, Table S3). We concluded, that Pou5f3 and Sox19b are dispensable for zygotic activation of maternal ß-catenin and Eomesodermin/FoxH1/Nodal targets.

25% of all zygotic transcripts repressed in the double mutant included BMP pathway components, the ventral targets of zygotic ß-catenin *vox, vent* and *ved* (Kawahara et

al., 2000; Melby et al., 2000; Shimizu et al., 2002; Varga et al., 2007; see Fig.5F), and multiple developmental regulators active throughout gastrulation (see Fig.S7A). The repression in the double mutants was in general non-additive (Fig. S7D), as expected when genes are activated by one of the two TFs.

Maternal Pou5f3 and Sox19b prevent the premature expression of late differentiation genes and restrict dorsal gene expression at ZGA

To take into account the transcripts present only in the mutants, we obtained the mutant time profiles with RNA-sense and scored the zygotic transcripts upregulated in the mutants at 5.5 hpf (Fig. 6A, Table S4). Zygotic transcripts, which were upregulated in single and double mutants, had elevated proportions of type 3 and type 4 enhancers within their putative regulatory regions (Fig. S7E). The group of 312 transcripts (all d>w, red frame in Fig. 6A) was synergistically upregulated in the double mutant (Fig.S7F) and strongly biased towards the developmental regulators, normally expressed during organogenesis (Fig. 6BC, Fig. S7G). The genes, prematurely activated in the double mutant, gained H3K27ac on their type 4 enhancers in both single mutants at dome stage (Fig.S7H). Taken together with the previous data, these results suggested that Pou5f3 and Sox19b synergistically prevent H3K27 acetylation and activation of two functionally distinct gene groups: the late developmental regulators and dorsal genes.

In zebrafish, similar to other vertebrates, the main product of Spemann's Organizer is Chordin, that blocks the flow of BMPs to the dorsal side of the embryo during gastrulation (De Robertis, 2009; Reid et al., 2012; Shimizu et al., 2000). Noggin1 redundantly supports the action of Chordin (Dal-Pra et al., 2006; Furthauer et al., 1999). The synergistic dorsalization in double mutants (Fig. 2C,D) could either result from early overexpression of Noggin1 (Fig.5B) or, alternatively, from the early misbalance between the dorsal and ventral gene regulatory networks, which converge on defining the relative size of the Chordin domain. To distinguish between these possibilities, we attempted to rescue M*sox19bspg* phenotypes by microinjecting Noggin1 or Chordin Morpholinos. The normal development of M*sox19bspg* could only be rescued by reduction of Chordin, but not of Noggin (Fig 6G). We concluded that synergistic activity of Pou5f3 and Sox19b at ZGA restricts Spemann organizer formation, by balancing the expression onset of multiple zygotic dorsal versus ventral developmental regulators at ZGA.

Discussion

Gene expression starts as a result of a multi-step regulatory programme, in which changes in chromatin accessibility, histone modifications and transcription quickly follow each other (Klemm et al., 2019). In this study, we dissected the contributions of Pou5f3 and Sox19b to each of these three steps during zebrafish ZGA. We found that Sox19b and Pou5f3 displace nucleosomes and promote H3K27 acetylation by binding to different cognate motifs (Fig.3G and Fig.4C). Sox19b and Pou5f3 directly activate 25% of early zygotic genes, by direct binding to two types of enhancers – Pou5f3-dependent type 1 and co-dependent type 2, which comprise 26% and 13% of all active enhancers at blastula stage, respectively. On type 2 enhancers Sox19b assists Pou5f3 loading, and Pou5f3 subsequently docks to the H3K27ac machinery (Fig.7A). The genes driven by type 2 enhancers are not expressed in MZ*sox19b* at least until the midgastrula (Fig. S5B), but this is dispensable for the gastrulation, as judged by the phenotypes of MZ*sox19b* mutant embryos and SoxB1 morphants (Fig.2B). We also define two types of enhancers, indirectly repressed by Pou5f3 and Sox19b, types 3 and 4.

Several novel insights to the regulatory landscape of the embryo are emerging from our study. First, maternal Pou5f3 and Sox19b synergistically restrict dorsal organizer at ZGA and are dispensable for the activation of Eomesodermin/FoxH1 targets (Fig.7B). Second, the antagonistic genome-wide effects of Pou5f3 and SoxB1 have to be balanced for proper ZGA timing (Fig.7C). Third, two groups of enhancers (types 3 and 4) are activated in the absence of Pou5f3 and/or Sox19b, which leads to premature activation of differentiation genes already at ZGA (Fig. 7DE).

Maternal Pou5f3 and Sox19b synergistically restrict dorsal organizer at ZGA and are dispensable for the activation of Eomesodermin/FoxH1 targets

In zebrafish, the initial establishment of the dorsal organizing center depends on the antagonistic activities of dorsal and ventral transcriptional repressors. Maternal β-catenin signaling directly induces the transcription factor Dharma/Bozozok at the dorsal side of the embryo (Fekany et al., 1999; Yamanaka et al., 1998). Dharma is repressed by zygotic ß-catenin signaling via its ventral targets, transcriptional repressors Vox, Vent and Ved. The mutual repression between Dharma and Vox, Vent and Ved defines the size of the dorsal organizer (Kawahara et al., 2000; Melby et al., 2000; Ramel and Lekven, 2004; Varga et al., 2007). The Eomes/FoxH1/Nodal pathway acts in parallel to Dharma to specify dorsal fates: organizer genes *noggin1, chordin* and *noto* are activated by both (Bruce et al., 2003; Koos and Ho, 1999; Reid et al., 2012; Sirotkin et al., 2000; Slagle et al., 2011), while *hhex* is a solely Dharma target (Bischof and Driever, 2004). It was previously shown that Pou5f3 directly activates *vox, vent* and *ved* on the ventral side (Belting et al., 2011; Reim and Brand, 2006), while Sox19b has the potential to repress Dharma and Nodal targets on the dorsal side of the embryo (Kuo et al., 2013; Shih et al., 2010). Synergy of these two effects at ZGA plausibly explains upregulation of *noggin1, noto and hhex* and severe dorsalization in the double mutants.

Zygotic transcription of the other known Eomes/FoxH1/Nodal targets, *sox32, mixl*, *sebox, foxa3, dusp4, chrd* and *tbxta*, is independent on Pou5f3 and Sox19b. These transcripts are first activated on the dorsal side of the embryo and/or in the extra-embryonic Yolk Syncytial Layer (YSL) (see Brown et al., 2008; Bruce et al., 2003; Du et al., 2012; Feldman et al., 1998; Hong et al., 2011; Nelson et al., 2014; Slagle et al., 2011). Taken together, these observations suggest that the establishment of

transcriptional competency at major ZGA is regional, mediated by different maternal TFs, priming distinct types of enhancers for activation on the dorsal and ventral sides of the embryo. Dorsal and mesendodermal genes are primed for activation by Eomesodermin, FoxH1 and probably Nanog. The broad range of other zygotic genes, including ventral and neuroectodermal genes, are primed for activation by Pou5f3 and Sox19b. This view is fully compatible with recent studies in mouse and Xenopus. In Xenopus, maternal Foxh1, together with two other maternal factors, bind to the endodermal enhancers prior to ZGA and primes them for zygotic activity (Charney et al., 2017; Paraiso et al., 2019). In mouse, Eomesodermin, together with Brachyury, are the solely responsible factors for establishing the competence for activation of mesodermal enhancers, and repress pluripotency and neuroectodermal programs, driven by Pou5f1 and Sox2 (Tosic et al., 2019).

Hidden Pou5f3/Sox19b antagonism underpins ZGA onset.

Ablation of maternal Sox19b or Pou5f3 results in the bulk non-specific delays of zygotic transcription and early development, most prominent in MZ*sox19b* (Movie S1, Fig.5D). ZGA timing is defined by competition between histones and transcription factors (Amodeo et al., 2015; Joseph et al., 2017; Wilky et al., 2019), and we expected that ablation of two major maternal TFs would additively delay ZGA. Surprisingly, we observed exactly the opposite: ZGA delays are compensated in the double maternal Pou5f3/Sox19b mutants (Fig.7C), revealing an antagonism between Pou5f3 and Sox19b “behind the scenes”. These results can be interpreted using a theoretical model, originating from analysis of Sox2 and Pou5f1 binding in ES cells (Biddle et al., 2019). The model predicts that two factors hinder each other’s binding across the genome in the majority of cases and help each other only in the minority of cases. Our finding that non-consensus binding of Pou5f3 and Sox19b results in the opposing changes on nucleosome landscape genome-wide (Fig.3F, Fig.S2) is compatible with this model. The majority of TF-DNA interactions, measured in single cell studies, have a very short residence time (e.g. 0.3 sec for Sox19b, Reisser et al., 2018), and were attributed to the non-consensus binding (Chen et al., 2014). Non-consensus binding is based on DNA shape features (Chiu et al., 2019; Samee et al., 2019) and changes the nucleosome occupancy genome-wide in different contexts (Afek et al., 2015; Veil et al., 2019). We speculate, that Sox19b and Pou5f3 may compensate most of each other’s effects across the genome by *i.e.* promoting displacement of the same nucleosome in the opposing directions, by recognizing different shape motifs within the same HNAR. In agreement with this hypothesis, SoxB1 and Pou5f3 tend to occupy different positions within HNARs: SoxB1 binds to the regions of higher *in-vitro* predicted nucleosome occupancy, than Pou5f3 (Fig. S1I). Interestingly, mammalian Sox2 and Pou5f1 binding on the nucleosome-wrapped DNA *in-vitro* show similar differences: Pou5f1 binds DNA at the entry- or exit- positions of the nucleosomes, SoxB1 proteins tend to bind closer to the nucleosome dyad (Zhu et al., 2018) and to the regions of higher predicted nucleosome occupancy (Li et al., 2019). In sum, we speculate that Pou5f3 and Sox19 mutually restrict each other’s genome-wide non-consensus effects on the nucleosome positioning, and this can be a general property of SoxB1 and PouV homologs across the organisms.

Pou5f3 and Sox19b balance the expression order of first and second periods of zygotic transcription (gastrulation/organogenesis).

We show that Pou5f3 suppresses H3K27 acetylation of SoxB1 target type 3 enhancers, and premature transcription of associated neural genes, normally expressed during organogenesis (Fig.7D). A similar phenomenon was recently documented in mouse ES cells, where Pou5f1 suppresses Sox2- dependent enhancers of neural differentiation genes (Friman et al., 2019). Another large group of late zygotic transcripts, enriched in regulators of differentiation and patterning for all tissues, is synergistically induced at the absence of both Pou5f3 and Sox19b (Fig. 6A, B, and Fig. 7E). Change of the early zygotic expression repertoire depends on activation of type 4 enhancers, which are silent at blastula stages during normal development (Fig. S7H). From the point of view of developmental logics, Pou5f3 and Sox19b ensure the proper time gap between the first and second periods of "morphogenetic nuclear activity" (Neyfakh, 1964), by shutting down the expression of genes which elicit later developmental programs. Balancing of early and late developmental programs by Pou5f3 and Sox19b provides a direct parallel to reprogramming in mouse fibroblasts, where Pou5f1 and Sox2 shut down the somatic gene expression programs and activate early embryonic genes (Chronis et al., 2017). At the moment, we have little idea of how they do it. Answering this question will require identification of TFs and chromatin modifiers, which promote H3K27ac on type 4 enhancers and activate transcription of the late genes at the absence of Pou5f3 and Sox19b. As the activation may be region-specific, these studies will require a combined single-cell analysis of transcription and enhancer accessibility.

Acknowledgments: We are grateful to Sebastian Arnold and Rainer Duden for commenting on the manuscript, to Sabine Götter for excellent fish care, and to Andrea Buderer and Cornelia Wagner for administrative support. D.O is especially grateful to Wolfgang Driever for hosting her lab. This work was supported by DFG-ON86/4-2 for DO, and DFG-EXC2189 – Project ID: 390939984 for D.O. and J.T. The Freiburg Galaxy Team is funded by DFG grant SFB 992/1 2012 and BMBF grant 031 A538A RBC**.**

Figures and Figure Legends

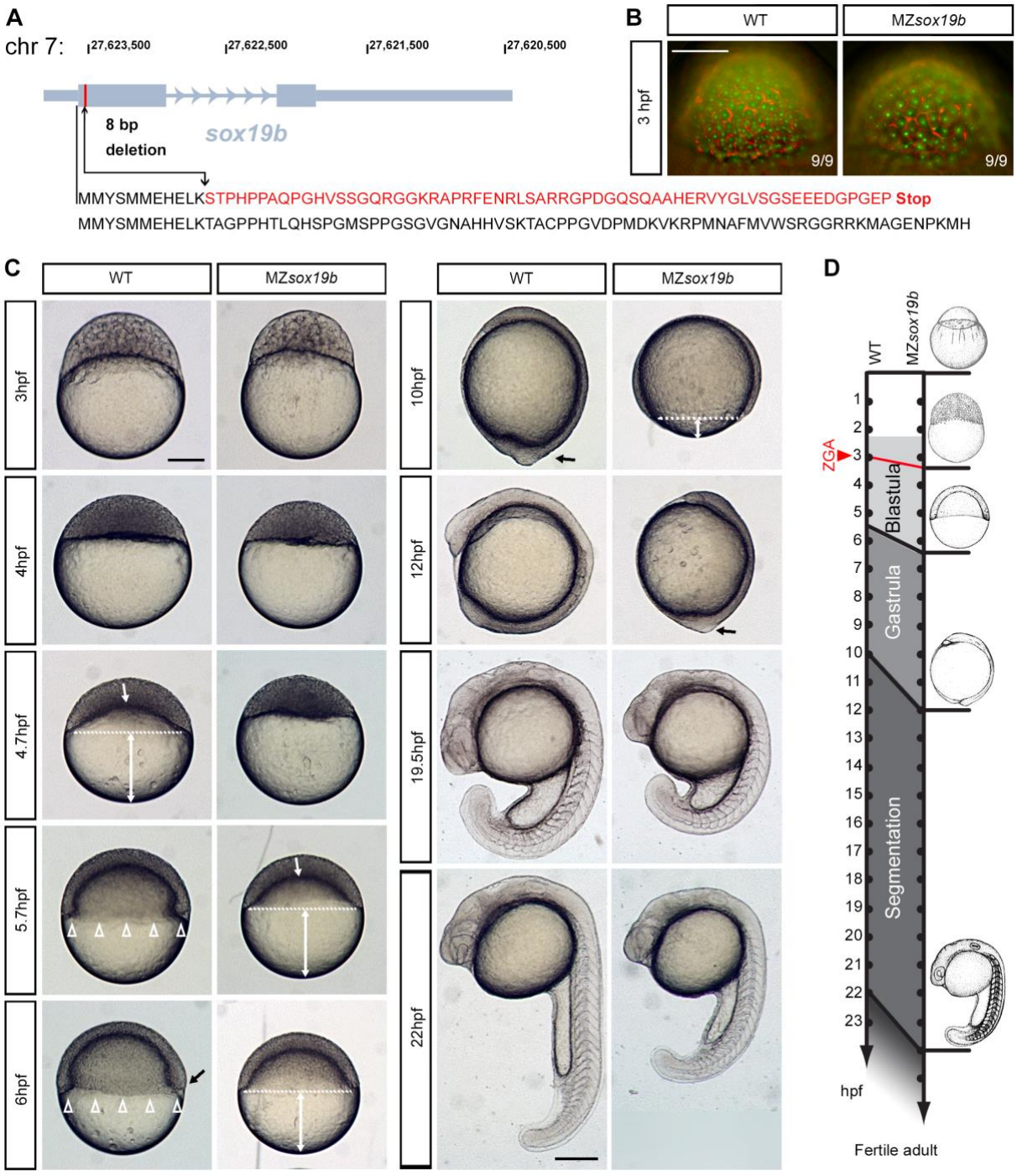

Figure 1: Mutation in maternal *sox19b* gene causes developmental delay starting at ZGA. A. Disruption of the *sox19b* gene on chromosome 7 by introducing an 8 bp deletion with TALEN technique. Mutation leads to a premature stop codon and thus a non-functioning protein. **B**. To determine when the time delay starts, we fixed WT and MZ*sox19b* embryos every 15 minutes starting from the 8th interphase (2.5 hpf to 4 hpf), and compared the cell size and nuclei number between the genotypes in each time point. First difference in cell size and nuclei number was detectable at 3.0 hpf (shown); indicating that when the WT embryos completed the 10th cell division, the MZ*sox19b* were still at 9th cell cycle. SYTOX green- nuclei, rhodamine-phalloidin- submembrane cytoskeleton. **C**. Phenotypes of the WT and MZ*sox19b* embryos at the indicated time points (hpf - hours post-fertilization), lateral views. Morphogenetic movements in

zebrafish blastula start from doming of the yolk (white arrow) followed by epiboly. Double white arrows show the distance from epiboly border (white dotted line) to the vegetal pole. At 4.7 hpf, when the wild-type embryos reach 30% epiboly, no doming could yet be seen in maternal zygotic Sox19b mutants (compare 4.7 hpf, and 5.7 hpf). Involution of mesendodermal layer marks gastrulation onset (hollow arrowheads in the wild-type, 5.7 hpf and 6 hpf), is followed by shield formation (black arrow in the wild-type, 6 hpf). The development of MZ*sox19b* embryos lags 45 min- to 1 hour behind that of the wild-type at 6 hpf. It takes 10 hpf for the wild-type and 12 hpf for MZ*sox19b* to complete gastrulation, which ends with tail bud formation (black arrow at 10 hpf, WT, and at 12 hpf in MZ*sox19b*). Scale bar 100 µm, stages as in (Kimmel et al., 1995). **D**. Altered developmental timing in MZ*sox19b*: 10th cell cycle is delayed at <=15 min, gastrulation starts 45 min-1 hour* later and completes 2 hours later than in the control.

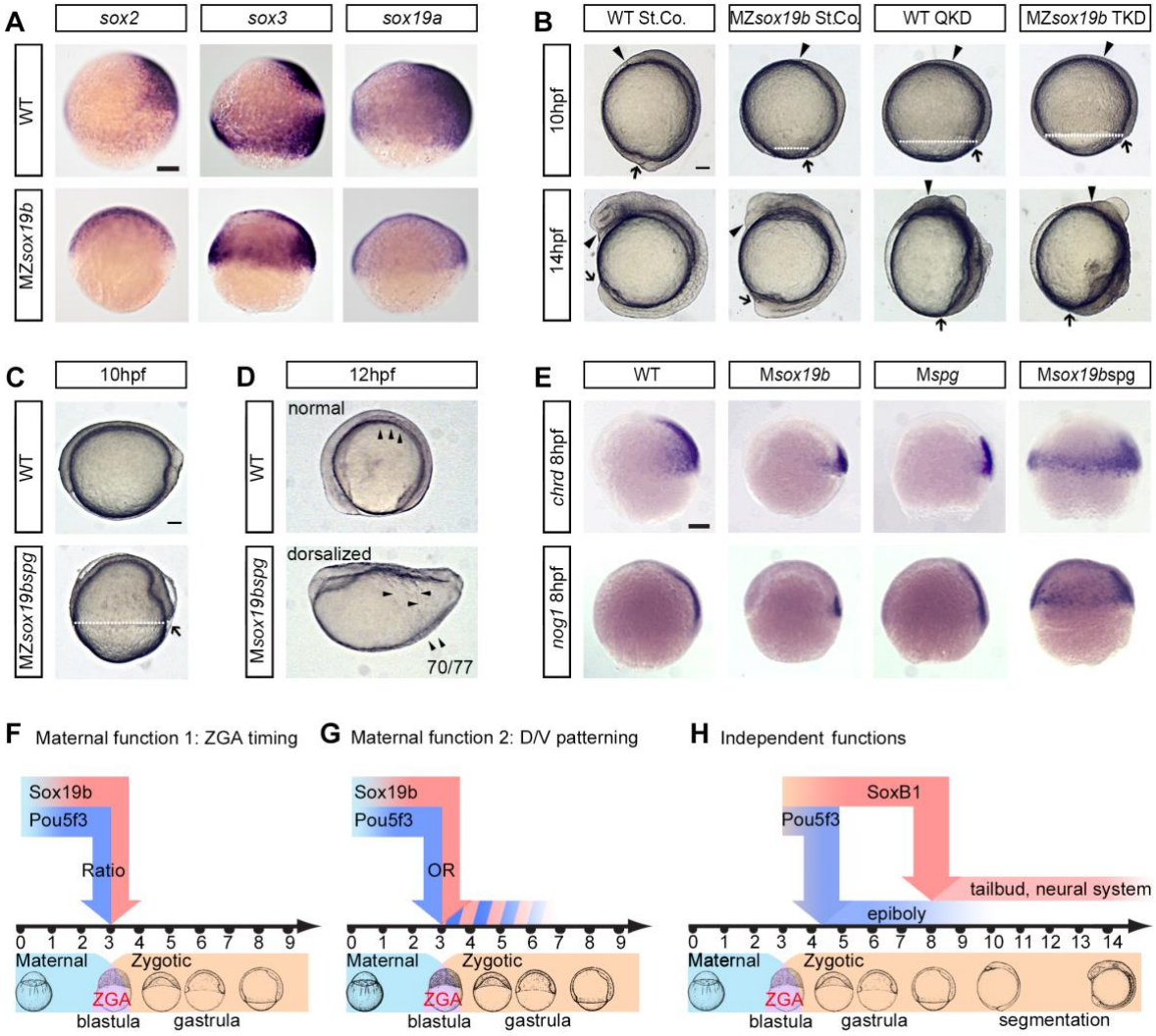

Figure 2: Biological functions of Sox19b and Pou5f3. A. Zygotic SoxB1 transcripts (*sox2, sox3 and sox19a*) are present in MZ*sox19b* mutant. Restriction of their expression to the neural part of the ectoderm occurs with a delay. *In situ* hybridization for zygotic soxB1 transcripts, lateral views, dorsal to the right, 8 hpf. **B.** SoxB1 knockdown embryos complete epiboly, but show defects in tailbud formation, A/P axis elongation and neural development. WT QKD- Quadruple morpholino injection into the wild-type knocks down *sox2, sox3 and sox19a/b*. MZ*sox19b* TKD - triple morpholino injection knocks down *sox2, sox3 and sox19a* in MZ*sox19b*. St. Co - standard control morpholino. Black arrow indicates shield or tailbud position; black arrowhead indicates the head position; epiboly border is shown as a white dotted line. **C**. Double maternal-zygotic Sox19b and Pou5f3 mutants MZ*sox19bspg* are arrested in epiboly and dorsalized. White dotted line shows epiboly border, arrow shows enlarged shield. **D.** Double Sox19b and Pou5f3 maternal mutants M*sox19bspg* +/- are dorsalized. Arrowheads show the borders of somites, normally forming on the dorsal side (WT), but spreading over the whole embryo in the M*sox19bspg*. The phenotype was observed in 70 out of 77 embryos which were alive at 12 hpf. Dorsal side up, anterior to the left. **E.** Simultaneous ablation of maternal Sox19b and Pou5f3 results in dorsalization, single ablations have no effect. *in-situ* hybridization for the Spemann Organizer transcripts *noggin1* and *chordin* in single and double maternal mutants, as indicated. Note that Spemann Organizer expands over the whole equatorial region in

the M*sox19bspg* double mutant embryos, but is rather reduced in the single mutants, when compared to the wild-type. **F-H.** Common and separate functions of Pou5f3 and Sox19b during the developmental periods indicated below the graph. **F.** Proper ratio of Pou5f3 and Sox19b at ZGA required for correct developmental timing. **G.** Either Sox19b or Pou5f3 should be maternally present in the embryo for correct D/V patterning. **G.** Pou5f3 is critical for epiboly during gastrulation, SoxB1 proteins are required for tailbud formation, A/P axis development and neural system formation after gastrulation. Scale bars in A-E: 100 µm.

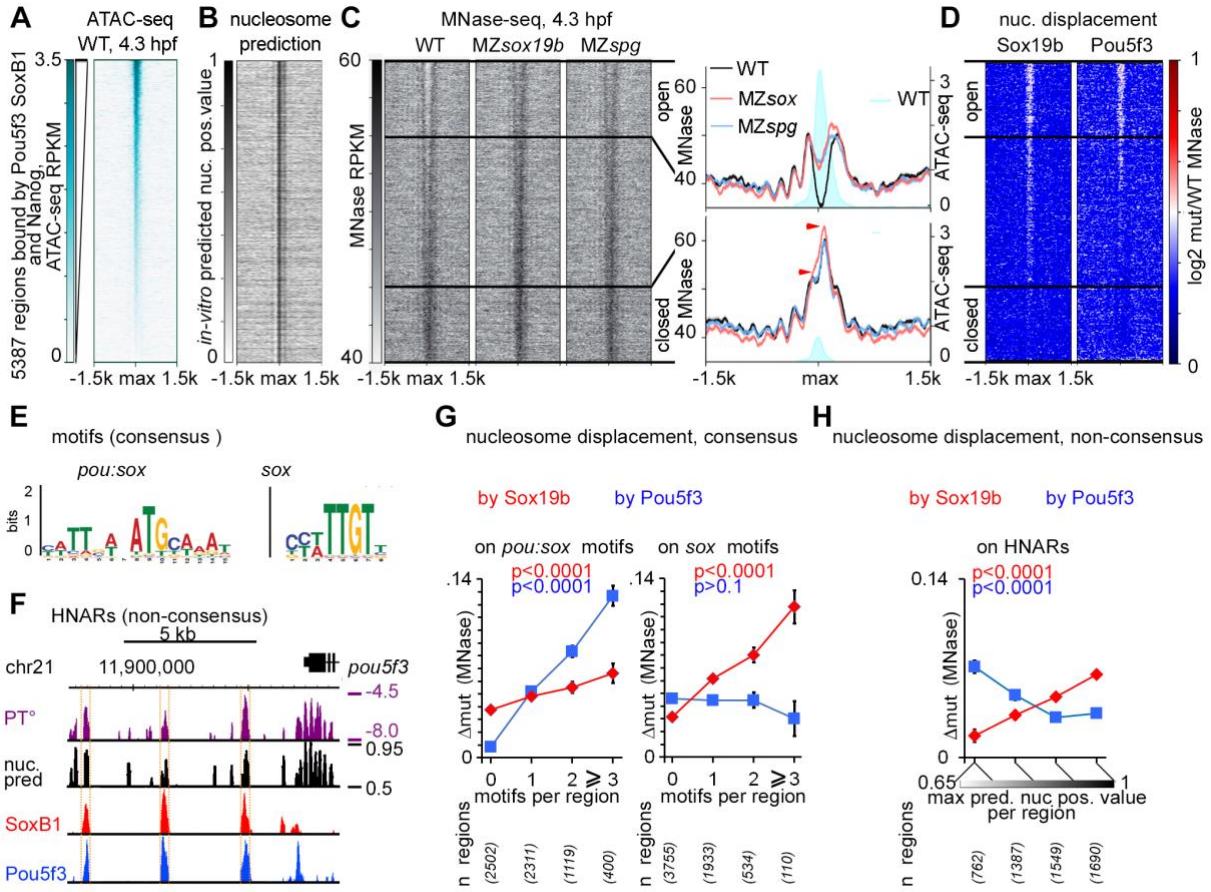

Figure 3: Sox19b and Pou5f3 bind independently across the genome. A-D. Heat maps of 5387 Pou5f3, SoxB1 and Nanog- bound (PSN) 3 kb genomic regions. The PSN-bound regions were aligned on max. *in-vitro* nucleosome prediction base pair within the central 320 bp ChIP-seq peak, oriented with higher *in-vitro* nucleosome prediction values to the right, sorted by descending ATAC-seq signal and extended to 1.5 kb from each side. **A.** ATAC-seq at 4.3 hpf (Liu et al. 2018), **B**. *in-vitro* predicted nucleosome occupancy. **C.** Left: experimental nucleosome occupancy at 4.3 hpf in the indicated genotypes (MNase-seq). Right: summary profiles of the nucleosome occupancy of the most "open" PSN bound regions versus the most "closed" (upper and lower quartiles when sorted by ATAC-seq signal). Note that the nucleosome occupancy of "closed" regions increases in MZ*sox19b* (red arrow heads), but not in MZ*spg*. **D**. Nucleosome displacement by each of the of two factors on HNARs can be directly visualized as a heat map of nucleosome occupancy difference between the respective mutant and the wild-type (log2 (mut/WT) MNase signal). **E** Consensus binding clues: *pou:sox* and *sox* motifs. **F.** Non-consensus binding clues: HNARs (genome browser view of three *pou5f3* enhancers). PT° - propeller Twist. **G**. Nucleosome displacement (by Sox19b (red) and Pou5f3 (blue) on PSN regions, depending on the number of *pou:sox* (left) and *sox* (right) motifs per region. Numbers of PSN genomic regions with 0,1,2 and 3 and more motifs are indicated below the graphs. **H.** Non-sequence specific (non-consensus) nucleosome displacement by Sox19b increases with the *in-vitro* predicted nucleosome positioning value of HNAR, Pou5f3 shows the opposite tendency. Nucleosome displacement by TF (Δmut (MNase) MZ*spg* and Δmut (MNase) MZ*sox19b)* was calculated as a normalized difference

between MNase signals in the respective mutant and the WT in the 0 to +150 bp region from the max. predicted nucleosome occupancy point. P-values for the 1-way ANOVA.

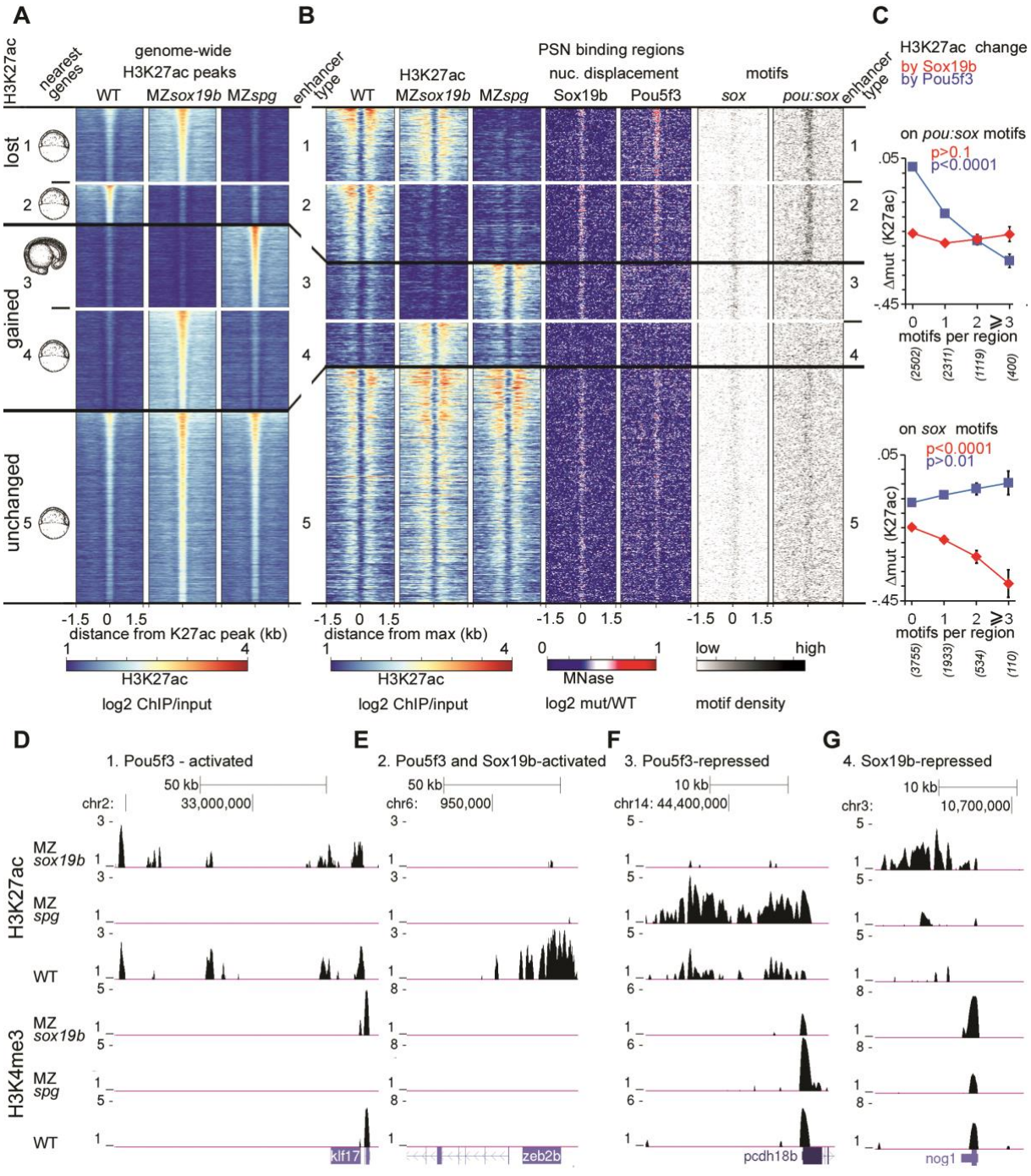

Figure 4: H3K27 acetylation is differentially regulated by Pou5f3 and Sox19b at four types of enhancers. A. 5 clusters of H3K27ac peaks: 1) lost in MZ*spg*, 2) lost in both mutants, 3) gained in MZ*spg*, 4) gained in MZ*sox19b* 5) unchanged. The icon at the left shows the developmental stage of expression (gastrulation or organogenesis) of associated genes enriched within each cluster. **B.** Heat maps of 5 enhancer types overlapping with PSN genomic regions, aligned on max. predicted nucleosome position of HNAR. Heat maps from left to right show H3K27ac signals in three mutants, nucleosome displacement in each mutant, and the density of motifs, as indicated. **C**. H3K27ac change by TF was calculated as a normalized difference between H3K27ac log2ChIP/input values (Δmut (K27ac) MZ*spg* and Δmut(K27ac) MZ*sox19b*) in the

respective mutant and the WT in the -500 to +500 bp region from the max. predicted nucleosome occupancy point. P-values for the 1-way ANOVA, numbers of genomic regions with 0,1,2 and 3 and more motifs are indicated below the graphs. **D-G.** Examples of top genes regulated by enhancer types 1-4 (UCSC genome browser, signal units are log2 ChIP/Input).

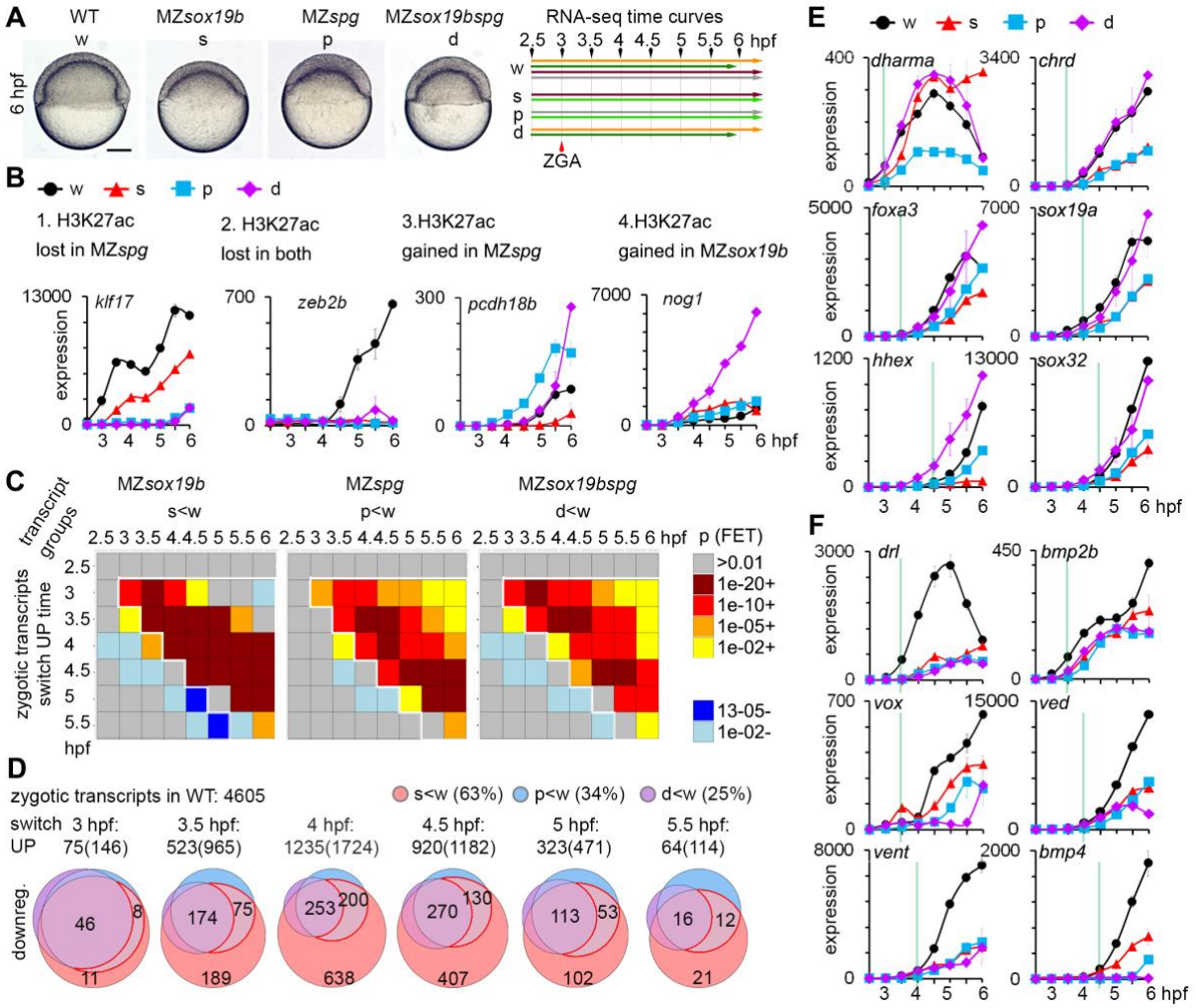

Figure 5: Direct activation of zygotic transcription by Pou5f3 and Sox19b is non-additive. A. Phenotypes of the maternal-zygotic Pou5f3 (p), Sox19b (s) and double mutants (d), compared to the wild-type (w) at 6 hpf. Right – RNA-seq experiments; samples collected in one experiment have the same color. **B.** Expression of the genes driven by enhancers type 1,2,3 and 4 in the WT, single and double mutants. **C.** RNA-sense correlation plots for zygotic genes downregulated in the indicated mutants. Y-axis - time profile groups by WT switch up time, X-axis – groups of downregulated transcripts (2 fold, p<0.001 in Student's T-test) per time point. FET- Fisher Exact Test. **D.** Venn diagrams show the overlaps of zygotic transcripts repressed in single and double mutants, per switch UP time group. Numbers above each diagram: n repressed transcripts (n total transcripts) per group. The zygotic transcript was scored as repressed, if it was downregulated at or after the switch UP point (to the right from the white line in C). Group of transcripts repressed in both single mutants, but not in double mutant (s,p<w) is highlighted by red frame. **E.** Maternal ß-catenin and Eomesodermin targets are not repressed in the double mutants (s,p<w group) **F.** Zygotic ß-catenin targets, BMPs and ventral marker *draculin* are repressed in single and double mutants (s,p,d<w group). RNA-sense switch up time point is indicated by green vertical line in E,F.

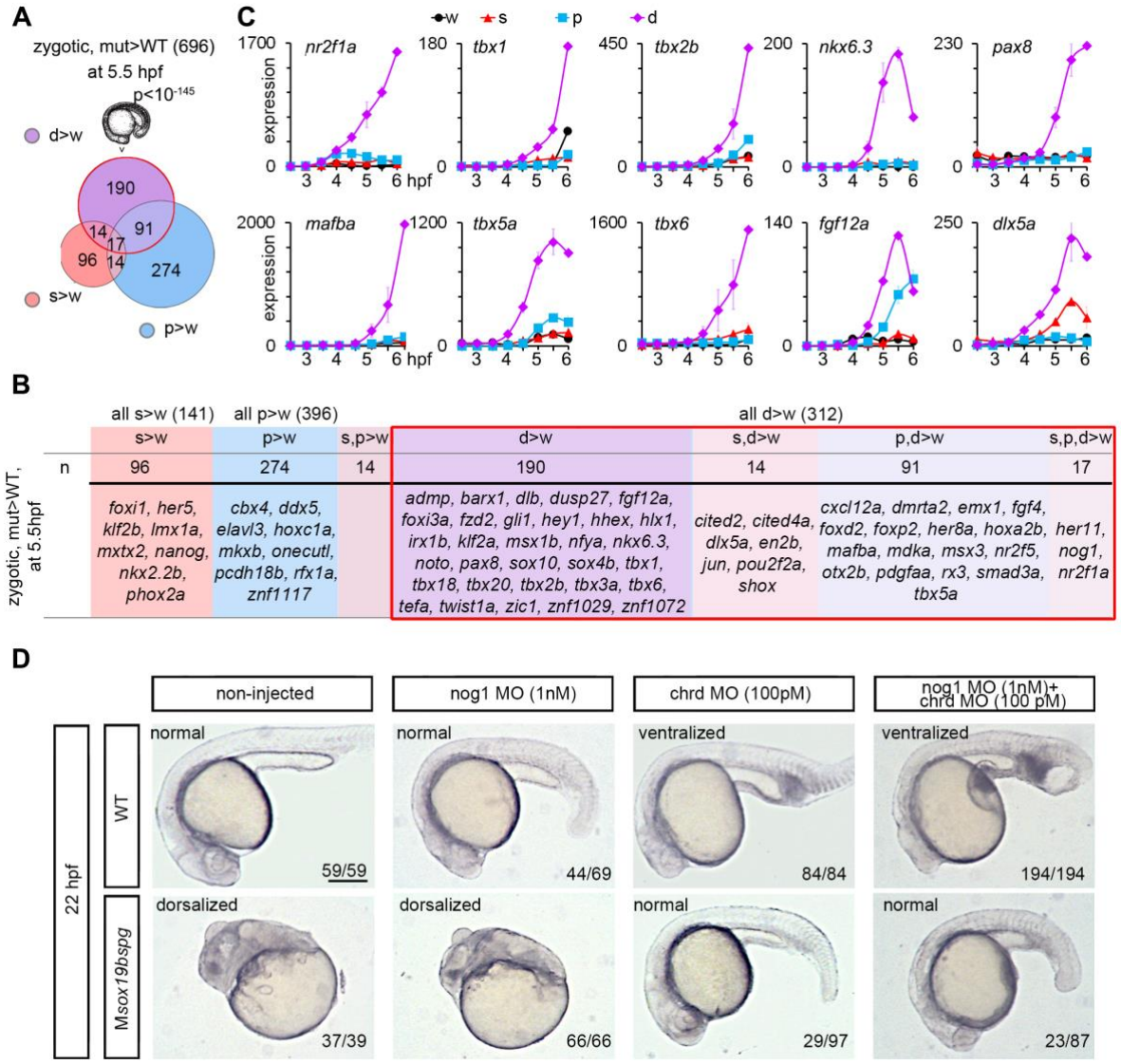

Figure 6: Pou5f3 and Sox19b synergistically repress differentiation regulators and dorsal genes. A,B. Groups of zygotic transcripts upregulated in one, two or three mutant backgrounds (s - MZ*sox19b*, p - MZ*spg*, d - MZ*sox19bspg*) at 5.5 hpf time point compared to the wild-type (w). Group of transcripts upregulated in the double mutant (all d>w) is highlighted by red frame. **A.** Venn diagram: transcripts upregulated in the double mutant are normally expressed during organogenesis stages (p - binomial p-value in GREAT, Hiller et al., 2013). **B.** Known developmental genes and transcription factors upregulated in the mutants, colors as in A. **C.** Premature induction of transcriptional regulators of organogenesis in the double mutant. **D.** Normal development can be rescued by reducing Chordin, but not Noggin levels in M*sox19bspg*+/- mutants. The wild-type or M*sox19bspg*+/- embryos were injected with the indicated morpholinos or non-injected. The numbers show the ratio of embryos with indicated phenotype/ all embryos alive at 22 hpf. The arrows show abnormally expanded blood progenitor cells in the ventralized wild-type embryos. Anterior to the left, dorsal up.

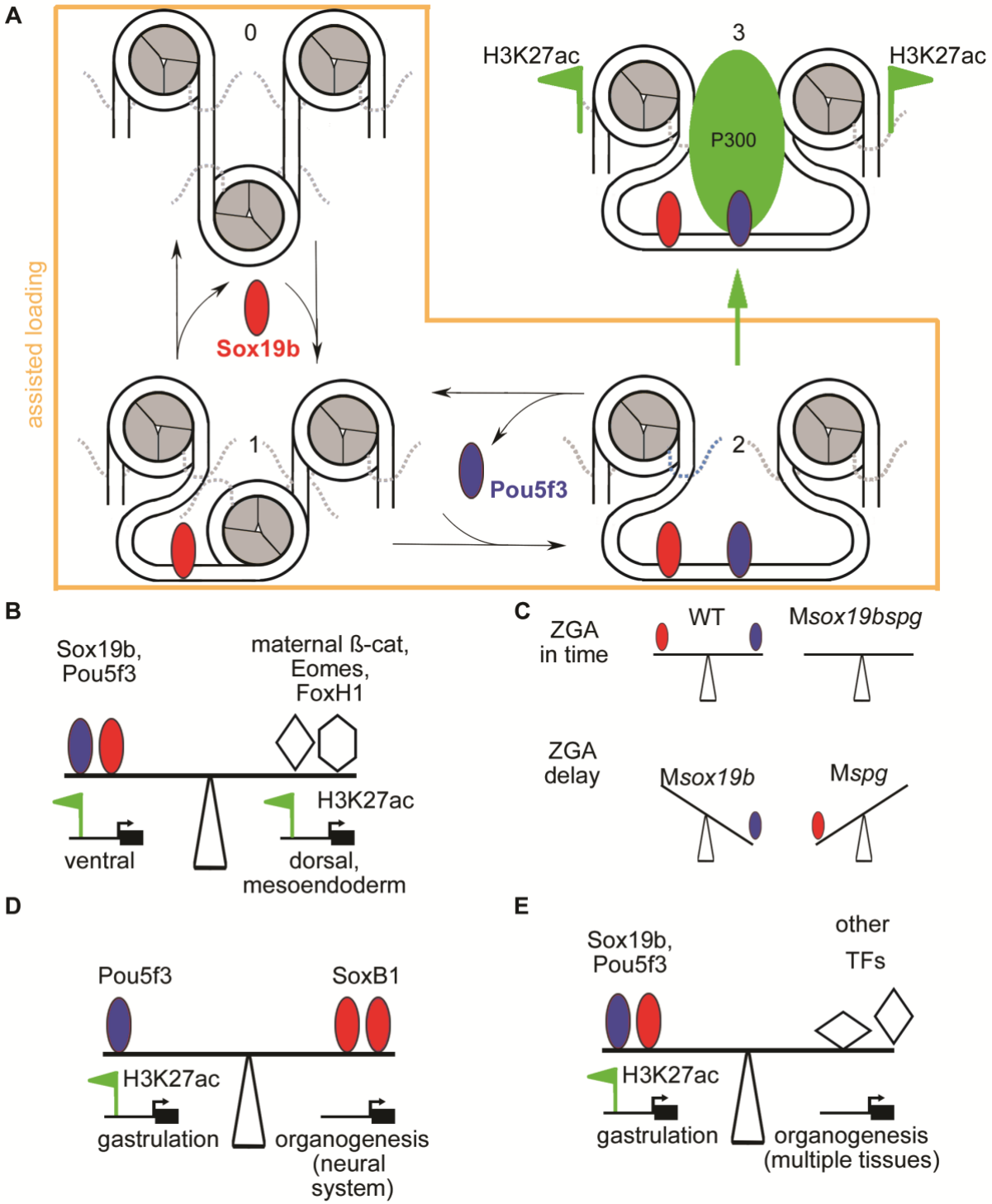

Figure 7: Summary of Pou5f3 and Sox19b activities. A. Sox19b-assisted Pou5f3 loading on co-dependent enhancers type 2. Sox19b competes with histones on *sox* motif (0-1), which allows Pou5f3 binding (2) to *pou:sox* motif nearby. (3): DNA-bound Pou5f3 promotes H3K27 acetylation of the neighboring nucleosomes**.** Green oval – P300. Nucleosome drawings are adapted from (Bowman and Poirier, 2015). **B.** The dorso-ventral balance at ZGA: Pou5f3 and Sox19b promote expression of the ventral genes via enhancers type 1 and 2, dorsal and mesendodermal are activated by maternal ß-cat, Eomesodermin and FoxH1 via enhancers type 4. **C.** The balance of Pou5f3 and Sox19b is important for bulk ZGA timing **D.** Pou5f3 activates gastrulation genes via enhancers 1 and 2 and indirectly suppresses premature expression of

organogenesis and neural differentiation genes by SoxB1 via enhancers type 3**. E.** The absence of both Pou5f3 and Sox19b results in premature activation of enhancers type 4, resulting in expression of multiple differentiation genes just after ZGA.

STAR+METHODS

KEY RESOURCES TABLE

REAGENT or RESOURCE	SOURCE	IDENTIFIER
Antibodies		
Anti-Histone H3 (acetyl K27) rabbit, 1/100 dilution	Abcam plc., Cambridge, UK	ab 4729
Anti-Histone H3 (tri-methyl K4) rabbit, 1/100 dilution	Millipore Co., Temecula, California, USA	07-449
Bacterial and Virus Strains		
One Shot™ TOP10 chemically competent *E. coli*	Invitrogen™	C404003
Chemicals, Peptides, and Recombinant Proteins		
cOmplete™, EDTA-free Protease Inhibitor Cocktail	Sigma-Aldrich Chemie GmbH, Germany	5056489001
Micrococcal Nuclease	Sigma-Aldrich Chemie GmbH, Germany	N3755-200UN
SYTOX Green	ThermoFisher SCIENTIFIC	S7020
Critical Commercial Assays		
Agencourt® AMPure® XP Beads	Beckmann Coulter, Krefeld, Germany	A63880
Agilent High Sensitivity DNA Kit	Agilent Technologies, Santa Clara, California, USA	5067-4626
Agilent RNA 6000 Nano Kit	Agilent Technologies, Santa Clara, California, USA	5067-1511
Dynabeads® Protein G	invitrogen Dynal AS, Oslo, Norway	10003D
E.Z.N.A® Cycle Pure Kit	Omega Biotek, Norcross, Georgia, USA	D6493-02
Microcon®-30 Centrifugal Filters	Merck Millipore, Darmstadt, Germany	MRCF0R030
mMESSAGE mMACHINE® SP6 transcription Kit	Ambion	10086184
NEBNext Ultra DNA Library Prep Kit for Illumina	New England Biolabs, Inc., Frankfurt a.M., Germany	E7370S
NEBNext® Multiplex Oligos for Illumina® (Index Primers Set 1)	New England Biolabs, Inc., Frankfurt a.M., Germany	E7335S
RNeasy® Mini Kit	QIAGEN, Hilden, Germany	74104
Quant-iT™ PicoGreen® dsDNA Assay Kit	invitrogen™ Molecular Probes® Waltham, Massachusetts, USA	Q33120
Deposited Data		
ATAC-seq of the WT 4.3 hpf zebrafish embryos	Liu et al. 2018	GEO: GSE101779
ChIP-seq for H3K27ac and H3K4me3 in three genotypes, 4.3 hpf	this work	GEO: GSE143306
ChIP-seq for Pou5f3 and SoxB1	Leichsenring et al., 2013	GEO: GSE39780
ChIP-seq for Nanog	Xu et al., 2012	GEO: GSE34683
ChIP-seq for Eomesodermin	Nelson et al., 2014	GEO: GSE51894

ChIP-seq for FoxH1	Dubrulle et al., 2015	GEO: GSE67648
Consensus *pou:sox* and *sox* motifs	Veil et al., 2019	Supplementary Table 2 in Veil et al., 2019
List of Pou5f3, SoxB1 and Nanog -bound and control genomic regions centered on HNARs (on max. nucleosome prediction within 320 bp around ChIP-seq peak) and oriented with min. nucleosome prediction to the left	Veil et al., 2019	Supplementary Table 1 in Veil et al., 2019
MNase-seq of MZ*sox19b* embryos, 4.3 hpf	this work	GEO: GSE125945
MNase-seq of WT and MZ*spg* embryos, 4.3 hpf	Veil et al., 2019	GEO: GSE109410
Time-resolved RNA-seq at 8 time points in 4 genotypes	this work	GEO: GSE137424
Zebrafish reference genome assembly danrer7/Zv9	Howe et al., 2013	http://genome.ucsc.edu/
Zebrafish reference genome assembly danrer11/ GRCz11	Genome reference Consortium	https://www.ncbi.nlm.nih.gov/grc/zebrafish
Experimental Models: Organisms/Strains		
Wild-type zebrafish strain AB/TL	ZIRC	ZL1/ZL86
MZ*spg* zebrafish	Lunde et al., 2004	m793
MZ*nanog* zebrafish	Veil et al., 2018	m1435
MZ*sox19b* zebrafish	this work	m1434
Oligonucleotides		
MO3-Sox2 Sox2 Morpholino 5' - GAAAGTCTACCCCACCAGCCGTAAA - 3'	Okuda et al., 2010	ZFIN ID: ZDB-MRPHLNO-080329-1
MO4-Sox2 Sox2 Morpholino 5' - GAGAGGCTGCTGAAGTTACCTTAGC - 3'	Okuda et al., 2010	ZFIN ID: ZDB-MRPHLNO-080329-2
MO3-Sox3 Sox3 Morpholino 5' - TACATTCTTAAAAGTGGTGCCAAGC - 3'	Okuda et al., 2010	ZFIN ID: ZDB-MRPHLNO-100527-3
MO4-Sox3 Sox3 Morpholino 5' - GAAGTCAGTCAAAAGTTCAGAGAGC - 3'	Okuda et al., 2010	ZFIN ID: ZDB-MRPHLNO-100527-4
MO1-Sox19a Sox19a Morpholino 5' - GTACATGGCTGCCAACAGAAGTTAG - 3'	Okuda et al., 2010	ZFIN ID: ZDB-MRPHLNO-100527-5
MO2-Sox19a Sox19a Morpholino 5' - AAAACGAGAGCGAGCCGTCTGTAAC - 3'	Okuda et al., 2010	ZFIN ID: ZDB-MRPHLNO-100527-6
MO1-Sox19b Sox19b Morpholino 5' - GTACATCATGCCACTTCTCGCTTTG - 3'	Okuda et al., 2010	ZFIN ID: ZDB-MRPHLNO-100527-7
MO2-Sox19b Sox19b Morpholino 5' - ACGAGCGAGCCTAATCAGGTCAAAC - 3'	Okuda et al., 2010	ZFIN ID: ZDB-MRPHLNO-100527-8
MOa-nog1 Noggin1 Morpholino 5' - GCGGGAAATCCATCCTTTTGAAATC - 3'	Dal-Pra et al., 2006	ZFIN ID: ZDB-MRPHLNO-080212-1
MO1-chrd Chordin Morpholino 5' - ATCCACAGCAGCCCCTCCATCATCC - 3'	Dal-Pra et al., 2006	ZFIN ID: ZDB-MRPHLNO-050221-6
PCR primer for genotyping Sox19b-f1 5'-ATTTGGGGTGCTTTCTTCAGC-3'	this work	no
PCR primer for genotyping Sox19b-r1 5'-GTTCTCCTGGGCCATCTTCC-3'	this work	no
PCR primer for ChIP-seq control, positive reference tiparp_f_1 5' CGCTCCCAACTCCATGTATC-3'	this work	no

PCR primer for ChIP-seq control, positive reference tiparp_r_1 5'-AACGCAAGCCAAACGATCTC-3'	this work	no
PCR primer for ChIP-seq control, negative reference igsf2_f_2 5'-GAACTGCATTAGAGACCCAC-3'	this work	no
PCR primer for ChIP-seq control, negative reference igsf2_r_2 5'-CAATCAACTGGGAAAGCATGA-3'	this work	no
Recombinant DNA		
CS2+Sox19b plasmid for mRNA synthesis	this work	no
Software and Algorithms		
Bed Tools	Quinlan and Hall,2010	BED Tools in usegalaxy.eu
Bowtie2	Langmead and Salzberg, 2012	Bowtie2 in usegalaxy.eu
DeepTools2	Ramirez et al., 2016	deepTools in usegalaxy.eu
DESeq2	Love et al., 2014	DESeq2 in usegalaxy.eu
FeatureCounts	Liao et al., 2014	featureCounts in usegalaxy.eu
Galaxy server	Afgan et al., 2018	https://usegalaxy.eu/
GREAT: Genomic Regions Enrichment of Annotations Tool, version 3.0.0	Hiller et al., 2013	http://great.stanford.edu/great/public-3.0.0/html/
In-vitro nucleosome prediction program	Kaplan et al., 2009 and https://github.com/bgruening/galaxytools	Nucleosome Predictions in usegalaxy.eu
k-means clustering algorithm	Ramirez et al., 2016	Available option in plotheatmap in deepTools2 in usegalaxy.eu
MACS2	Ferg et al., 2007	MACS2 callpeak and MACS2 bdgpeakcall in usegalaxy.eu
RNA Star	Dobin et al., 2013	RNA Star in usegalaxy.eu
RNA-sense	this work	https://bioconductor.org/packages/release/bioc/html/RNAsense.html

LEAD CONTACT AND MATERIALS AVAILABILITY

Requests for zebrafish lines and reagents generated in this study should be directed to and will be fulfilled by the Lead Contact, Daria Onichtchouk: daria.onichtchouk@biologie.uni-freiburg.de

EXPERIMENTAL MODEL AND SUBJECT DETAILS

Wild-type fish of AB/TL and mutant sox19b^{m1434} strains were raised, maintained and crossed under standard conditions as described by Westerfield (Westerfield, 2000). The mutant spg^{m793} line were maintained as described previously (Lunde et al. 2004). Embryos obtained from crosses were collected within 10 minutes and raised in egg water at 28.5°C. Staging was performed following the Kimmel staging series (Kimmel et al., 1995). Stages of the mutant embryos were indirectly determined by observation of wild-type embryos born at the same time and incubated under identical conditions. All experiments were performed in accordance with German Animal Protection Law (TierSchG).

sox19b TALEN mutagenesis

To generate a *sox19b* zebrafish mutant, we used the TALEN technique and targeted the first exon for the mutation. The square brackets indicate the spacer sequence, flanking sequences should bind to TAL1 and TAL2 (Cermak et al., 2011): 5'-GATGGAGCACGAGCT[GAAGACCGCTGGTCCA]CCCCACACCCTCCAGC-3' (according to assembly Jul. 2010, zv9/danRer7). For restriction digest the enzyme BbsI was selected with the corresponding restriction site 5'-GAAGAC-3'. After injecting the TALENs (100 ng/µl each) into one-cell stage wild-type embryos we tested the proper activity of TALENs. We extracted genomic DNA from 20 of 24 hpf old WT and 20 injected embryos by lysing the cells with lysis buffer (10 mM Tris pH 8, 50 mM KCl, 0.3% Tween20, 0.3% NP-40, 1mM EDTA) and incubated the embryos at 98°C for 10 min. After cooling down Proteinase K solution (20 mg/ml, A3830, AppliChem) was added and incubated over night or at least 2 hours. Subsequently the Proteinase K was destroyed by heating up to 98°C for 10 min. We used the following primers for PCR: Sox19b-f1 5'-ATTTGGGGTGCTTTCTTCAGC-3' and Sox19b-r1 5'-GTTCTCCTGGGCCATCTTCC-3'. This gives a product of 362 bp length. This product contains two restriction sites for BbsI, so we got after digestion overnight three bands with sizes of 40 bp, 132 bp and 190 bp in which the 40 bp band also appears in wild-type embryos. After successful TALEN injection we let the fish grow and found through an outcross with wild-type two founders out of 19 tested fishes. From these two founders we chose the one with an 8 bp deletion resulting in a frameshift and a stop codon after 62 amino acids (5'-GATGGAGCACGAGCTGAAGA|CCACCCCACACCCTCCAGC-3', the line shows the position where the deletion occurred). For further experiments we used then the offspring with this mutation.

Morpholino knockdown

Two translation-blocking morpholinos for each of *sox2*, *sox3*, *sox19a* and *sox19b* were designed by Okuda (Okuda et al., 2010). All morpholinos were provided by Gene Tools. LLC (Philomath, USA). To generate SoxB1 knockdown embryos, 1.8 ng of morpholino mix for SoxB1 gene was microinjected into 1-cell stage embryos. For TKD 5.4 ng of standard control morpholino was taken, while 7.2 ng of standard morpholino was injected as QKD control. Noggin and Chordin Morpholinos were designed by Dal-Pra et al (2006). To block Noggin translation, 1 nM Noggin MO was injected. To moderately Chordin translation, 100 pM Chordin Morpholinos were injected, as recommended by Dal-Pra et al. (2006).

Rescue of MZ*sox19b* TKD with *sox19b* mRNA

Sox19b open reading frame was amplified from zebrafish total cDNA (4.3 hpf), using primers designed according to *sox19b* mRNA sequence in UCSC. The PCR product was cloned in pCRII-TOPO vector with TOPO TA Cloning® Kit (Invitrogen) following the manual, and then sub-cloned into PCS2+ vector. mRNA was *in-vitro* transcribed with mMESSAGE mMACHINE® SP6 Kit (Ambion) according to the user's manual. Sox19b mRNAs were cleaned up with QIAGEN RNeasy® Mini Kit and 20 pg per embryo was co-injected into 1-cell stage embryo together with TKD Morpholinos.

Cell division counting in living embryos

SYTOX Green (0.2 mM, ThermoFisher SCIENTIFIC) mixed with 0.2 M KCl and 1 nl was injected in wild-type and *MZsox19b* mutant embryos at the 1-cell stage. Embryos which showed a proper SYTOX Green fluorescence were selected under the fluorescence stereomicroscope and placed in a furrow of an agarose plate. They were covered with a 24 x 60 mm cover slide which was fixed with 2% low melting agarose and overlaid with 0.3x Danieau's buffer to prevent drying out of the embryos. Subsequently the development of the embryos was documented by using Leica MZ16 FA Fluorescence Stereomicroscope and Leica Microsystems LAS AF software which took every 3 min a bright field image and a fluorescent image (GFP filter, 395 nm). The temperature during documentation was 24°C. Resulting images were analyzed with ImageJ by counting the single images between mitoses. The obtained number of images was multiplied with 3 min to achieve the time span in minutes between the cell divisions.

Live imaging

Zebrafish embryos were imaged according to the wild-type control stages under Leica MZ APO stereomicroscope using AxioVision SE64 Rel. 4.9.1 software, with 50x magnification for single embryo and 12.5 x magnifications for the overview. Photos were arranged in Adobe Photoshop CS5.

Time-lapse imaging

Wild type and mutant embryos were collected at the same time and dechorionated manually in 0.3x Danieau's buffer. Then one embryo from each genotype was picked and placed on a 1.5% agarose chamber filled with 0.3x Danieau's buffer. Images were taken with 3 min interval for 24 hours by either Leica MZ APO stereomicroscope using AxioVision SE64 Rel. 4.9.1 software, or The IMAGINGSOURCE DFK21F04 with IC capture ver 2.3.394.1917. Room temperature was kept at 26-28°C during the documentation. Images were further processed in ImageJ 1.50i.

Whole mount *in situ* hybridization (WISH)

To visualize the expression pattern of some chosen genes we performed whole mount in situ hybridization as previously described (Veil et al., 2018). The plasmids for anti-sense RNA probe synthesis were kind gifts of Wolfgang Driever, Matthias Hammerschmidt, Yusuke Kamachi and Liliana Solnica-Krezel. Embryos were fixed at proper stages with 4% paraformaldehyde at 4°C overnight, 3 times washed in PBST for 5 min, dechorionated manually in PBST and dehydrated with ascending series of methanol to 100%. Embryos in 100% methanol were stored at -20°C. After rehydrating with descending series of methanol to PBST, embryos were washed 3 times in PBST, pre-hybridized in 300µl Hyb-Mix for 3 hours at 65°C. 2 µl of prepared probes were added to 300µl Hyb-Mix for hybridization overnight at 65°C. Emrbyos were placed into 24-well plates and washed with in situ robot BioLane™ HTI by series washing steps: firstly embryos were washed three times for 20min in 300 µl 50% Formamide at 65°C, in 500 µl 2x SSCT for 15 times at 65°C, three times in 500 µl 0.2x SSCT for 20 min at 65°C, twice in 1 ml PBST for 10 min at room temperature. Then embryos were incubated in blocking solution (2% goat serum (heat inactivated) in PBST/BSA (2 mg/ml) for 2 hours at RT and incubated overnight with anti-DIG (1:5000 diluted in PBST) at 4°C. After washing 6 times for 20 min in 1ml PBST and once for 10min in 100Mm Tris-HCl, (pH=9.5), embryos were incubated with staining buffer for 15 min and the robot program is finished. We replaced staining buffer with 500 µl staining solution and stained for a proper time on a shaker. To stop the staining process embryos were washed with stop solution. Stained embryos were fixed in an increasing series of glycerol (25%, 50% and 75% in PBST), finally stored in 100% glycerol at 4°C. These embryos were imaged with Leica MZ APO stereomicroscope using AxioVision SE64 Rel. 4.9.1 software and the images were processed in Adobe Photoshop CS4.

MNase-seq, data processing and visualization.

MNase-seq and data processing was performed as previously described (Veil et al., 2019). Briefly, 200-400 MZ*sox19b* embryos were dechorionated and fixed 10 minutes in 1% Formaldehyde at dome (4.3 hours post-fertilization) stage. The nuclei were isolated and digested with MNase. The yield of and degree of digestion was controlled using Agilent High Sensitivity DNA Kit on Agilent Bioanalyzer, according to manufacturer instructions. Chromatin was digested so that it contained 80% mono-nucleosomes. Libraries were prepared using the Illumina sequencing library preparation protocol and single-end sequenced on an Illumina HiSeq 2500 by Eurofins Company (Germany). All further data processing was done using European Galaxy server usegalaxy.eu (Afgan et al., 2016). Sequenced reads were mapped to the zebrafish danrer7/Zv9 assembly (Howe et al., 2013) using Bowtie2 (Langmead and Salzberg, 2012). Resulting BAM files were converted to BED format, all mapped reads were extended to 147 bp in their 3' direction, truncated to the middle 61 bp and converted back to BAM format using BED Tools (Quinlan and Hall, 2010). To create Bigwig files for the visualization of nucleosome density, BAM files for MZ*sox19b* (this work), MZ*spg* and WT (Veil et al., 2019) were normalized to rpkm (reads per million reads per one kilobase) and converted to bigwig format using BAM coverage program in deepTools (Ramirez et al., 2016). To create Bigwig files for the visualization of nucleosome displacement by Sox19b and Pou5f3, the log2 ratio of nucleosome occupancy (in rpkm) between each mutant and the wild-type was obtained using BAM compare program in deepTools. The heatmaps or profiles of selected genomic regions were plotted using plotheatmap or plotprofile programs in deepTools (main Fig. 3CD, Fig. 4B, Fig. S1G, Fig. S2E-G).

ChIP-seq for chromatin marks

The freshly laid eggs of MZ*sox19b*, MZ*spg* mutants and wild-type were collected in 10-15 min intervals. Unfertilized eggs were removed at 2-4 cell stage. Collected embryos were transferred to 0.5x Danieau's solution (for 1L of 30X stock: 1740 mM NaCl, 21 mM KCl, 12 mM MgSO4, 18 mM Ca(NO3)2, 150 mM HEPES buffer, ph 7.6; dilute 60X before use) (Westerfield, 2000) followed by enzymatic dechorionation with pronase E (0.3 mg/ml). The reaction was stopped by adding 1 % BSA (final conc. 0.04 %) followed by two to three washing steps with 0.5x x Danieau's. The eggs were cultured in glass petri dishes to prevent the embryos from adhere to the dish and thus eventually rip. They were incubated at 28 °C until the 4.3 hpf stage was reached. In order to fix the chromatin state at developmental stage 4.3 hpf (dome) and avoid nucleosome shifts, the dechorionated embryos were homogenized in 10 ml 0.5 % Danieau's

containing 1x protease inhibitor coctail (PIC) using a Dounce tissue grinder and immediately treated with 1 % (v/v) Methanol-free Formaldehyde (Pierce) for exactly 10 min at room temperature. The homogenizate was transferred into a 15 ml falcon tube and shaken on a rotating platform for the rest of the 10 min. The fixation was stopped with 0.125 M Glycine by shaking for 5 min on a rotating platform. Subsequently the homogenizate was centrifuged for 5 min, 4700 rpm at 4 °C, whereupon a white pellet formed. The supernatant was discarded, and the pellet was resolved in Wardle cell lysis buffer (10 mM Tris-HCl (pH 7.5), 10 mM NaCl, 0.5 % NP-40, 1-4 ml/1000 embryos). The lysate was distributed upon 2 ml eppendorf tubes, followed by 5 min incubation on ice with subsequent 1 min centrifugation, 2700 g at 4 °C. The supernatant was discarded again and the pellet was washed 2 times with 1 ml ice cold 1x PBST (for 1 L: 40 ml PO4 buffer (0.5 M), 8 g NaCl, 0.2 g KCl, 0.1% Twen20, pH 7.5). In order to count the obtained nuclei, the pellet was resolved in 1 ml ice cold 1x PBST, of which 10 µl were diluted 1:1 with Sytox® green (1:400) and fluorescence microscope examined by using the Neubauer counting chamber. The obtained amount of nuclei was calculated using the following equation:

Nuclei/(µl)=(number of counted nuclei)/(〖counted area (mm〗^2)* chamber depth (mm)*dilution)

The residual nuclei were again pelleted by 1 min centrifugation at 2700 g and 4 °C, subsequently snap frozen in liquid nitrogen and stored at -80 °C. 2.5 million nuclei were used to perform one ChIP-Seq experiment.

The chromatin was thawed and resolved in 2 ml of Wardle nuclei lysis buffer (50 mM Tris-HCl (pH 7.5), 10 mM EDTA, 1 % SDS) and incubated 1 h on ice. In order to shear the chromatin to 200 bp fragments (on average), the chromatin was sonicated using the Covaris S2 sonicator (DC 20 %, Intensity 5, Cycles of Burst 200, Time = 3*40 cycles with 30 sec each (3*20 min)). To ensure that the sonication was successful, 30 µl of the sheared chromatin was de-crosslinked with 250 mM NaCl over night at 65 °C and then analyzed using the Agilent Expert 2100 Bioanalyzer® and Agilent high sensitivity DNA Chip kit.

The lysed and sheared samples were centrifuged for 10 min at 14,000 rpm and 4 °C. 60 µl of each sample were kept as input control. The chromatin was then concentrated to 100 µl using the Microcon centrifugal filters (Merck Millipore MRCF0R030) and diluted 1:3 by adding ChIP dilution buffer (16.7 mM Tris-HCl pH 7.5, 167.0 mM NaCl, 1.2 mM EDTA) containing protease inhibitors. 3 µg of referring antibody were added and incubated overnight at 4 °C on a rotating wheel.

150 µl of magnetic Dynabeads coupled to protein G (Stock 30 mg/ml; invitrogen DynaI 10003D) were transferred into a 2 ml eppendorf tube and placed on a magnetic rack in order to remove the liquid from the beads. Subsequently the beads were washed 3x with 5 mg/ml specially purified BSA in PBST and 1x with 500 µl ChIP dilution buffer. After removing the ChIP dilution buffer, the chromatin-antibody mix was added and incubated with the beads at 4 °C overnight on a rotating wheel.

Beads were pulled down by placing the eppendorf tubes on the magnetic rack in order to discard the supernatant. The beads were resuspended in 333 µl RIPA buffer containing PIC. The Protein G-antibody-chromatin complex was washed 4x5 min on a rotating platform with 1 ml of RIPA buffer (10 mM Tris-HCl (pH 7.6), 1 mM EDTA, 1 % NP-40, 0.7 % sodium deoxycholate, 0.5M LiCL), followed by 1x1 ml TBST buffer (25 mM Tris-HCl,150 mM NaCl, 0.05% Tween 20, pH 7.6). The beads were pulled down again and the supernatant was removed. In order to elute the chromatin, 260 µl elution buffer (0.1 M NaHCO3, 1% SDS) was added and incubated for 1 h at 65 °C in a water bath. The samples were vortexed every 10 - 15 min. Afterwards the supernatant was transferred to a fresh eppendorf tube by pulling the beads down, using the magnetic rack. 12.5 µl 5M NaCl was added to de-crosslink the chromatin and incubated overnight at 65 °C in a water bath. The input samples were treated as control in parallel (230 µl elution buffer per 30 µl input).

Purification of the de-crosslinked chromatin was performed using the QIAquick PCR Purification Kit from Qiagen. The concentration was determined using the Qubit fluorometer and Quanti-iT™ PicroGreen® dsDNA Kit according to manufacturer instructions.

To validate if ChIP experiments were successful, we performed quantitative PCR in ChIP and Input control material, using the primers for the positive and negative reference genomic regions, enriched in or devoid of chromatin marks (see KEY RESOURCES TABLE). According to previously published data, the chromatin region near *tiparp* gene was highly enriched in H3K27ac and H3K4me3 histone marks at 4.3 hpf, while genomic region near *igsf2* gene did not bear any of these mark (Bogdanovic et al., 2012). QPCR was carried out using the SsoAdvanced™ Universal SYBR® Green Supermix from BIO-RAD. ChIP and input were normalized using negative reference region *(igsf2*). The ChIP experiment was

considered successful, if the enrichment in ChIP over input control on the positive reference region (*tiparp*) was more than 5-fold.

In order to convert a small amount of DNA into indexed libraries for Next Generation Sequencing (NGS) on the Illumina platform we used the NEBNext® Ultra™ DNA Library Prep Kit according to manufacturer instructions, with the modifications indicated below. The library preparation follows a 4-step protocol including end-repair (5' phosphorylation, dA-tailing), adaptor ligation, PCR enrichment including barcoding and clean up. Since the DNA input was <100 ng, in the adaptor ligation step, the NEBNext Adaptor for Illumina® (15 µM) was diluted 10-fold in 10 mM Tris-HCl (pH 7.8) to a final concentration of 1.5 µM and used immediately. At the final clean-up step, the reaction was purified by mixing the samples with AMPure XP Beads (45 µl) before incubating at room temperature for 5 min. After a quick spin using the tabletop centrifuge, samples were placed on a magnetic rack and supernatant was discarded. 200 µl of 80 % Ethanol were added and removed after 30 sec, two times. The beads were air dried for 3 min. and the DNA target was subsequently eluted by adding 33 µl of 0.1x TE (pH 8) and incubation at room temperature for 2 min. 28 µl of the library were transferred to a fresh PCR tube and stored at -20 °C. 2 µl of the sample were diluted 5-fold with 0.1x TE and used to check the size distribution of the library using Agilent Expert 2100 Bioanalyzer® and Agilent high sensitivity DNA Chip kit. In order to reduce the peak of residual unligated Adaptors, the reaction was re-purified, by adding H2O up to 50 µl and 45 µl of AMPure XP Beads. The concentration was determined using the Qubit™ Fluorometer and Quanti-iT™ PicroGreen® dsDNA Kit. The 7 ChIP-seq libraries were sequenced at 70 mln paired end 150bp reads each: WT K27ac Chip, MZ*spg* K27ac Chip, MZ*sox19b* K27ac Chip1, MZ*sox19b* K27ac Chip2, WT K4*me3* Chip, MZ*spg* K4me3 Chip, MZ*sox19b* K4me3 Chip. The 7 corresponding input libraries were sequenced to 30 mln reads in the Novogene company (China).

Chromatin ChIP-seq data analysis

H3K27ac and H3K4me3 ChIP-seq data processing was done using european Galaxy server usegalaxy.eu (Afgan et al., 2016). Sequenced reads were mapped to the zebrafish danrer7/Zv9 assembly (Howe et al., 2013) using Bowtie2 (Langmead and Salzberg, 2012). Peak calling was performed using MACS algorithm (Feng et al., 2012)). To reduce the number of false positives, peak calling for each H3K27ac ChIP-seq experiment (WT K27ac Chip, MZ*spg* K27ac Chip, MZ*sox19b* K27ac Chip1, MZ*sox19b* K27ac Chip2) was performed five times: peaks were called using four different background files (with the application MACS2 callpeak), or without background (with the application MACS2 bgpeakcall). Only H3K27ac peaks present in all five peak calls were kept for further analysis. For MZ*sox19b* ChIP-seq, only the peaks present in both biological replicates were taken. H3K4me3 peaks were called once with the application MACS2 bgpeakcall. On the next step, H3K27ac or H3K4me3 peaks from different genotypes were piled together and the overlapping regions were merged. To obtain the common list of putative H3K27 acetylated enhancers in all genotypes, the H3K27ac peaks which overlapped with H3K4me3 peaks were removed. The resulting list in BED format was sorted according to descending peak strength. To create Bigwig files for the visualization of histone mark levels and for k-means-clustering, the log2 ratio between each ChIP and corresponding input (in rpkm) was obtained using BAM compare program in deepTools (Ramirez et al., 2016). For MZ*sox19b*, one of the two biological replicates (rep.1) was used. Unsupervised clustering was performed with k-means algorithm within plotheatmap program in deepTools. The heatmaps or profiles of H3K27ac levels on selected genomic were plotted using plotheatmap or plotprofile programs in deepTools (Fig.4A,B, Fig.S3). Histone modification profiles in single genes (Fig. 4 D-G, Fig. S4, Fig.S7H) were visualized using UCSC browser.

GREAT analysis, "top enhancer type" genes

GREAT analysis (Hiller et al., 2013) of genomic regions matching to H3K27ac ChIP-seq peaks of clusters 1 to 5 was performed at http://great.stanford.edu/great/public-3.0.0/html/ . Genomic regions were associated with genes using 20 kb single nearest gene association rule. The genes, associated with the highest number of peaks of clusters 1-4 (Table S2), were visually checked in UCSC browser and selected as " top enhancer type 1-4" genes.

Motif analysis.

Position-weight matrices for *sox* and *pou:sox* motifs from the Supplementary Table 2 in Veil et al., 2019, were used. Genomic coordinates of the individual motif occurrences in +/- 1.5 kb from the center of selected genomic regions were obtained using FIMO (Grant et al. 2011) with p-value threshold 10^{-4}. The genomic coordinates of motifs were saved as a BED file, converted to Bigwig format with BEDTools

(Quinlan and Hall 2010), and used for visualization of the motif density on the selected genomic regions (Fig.4B, Fig.S1H, Fig.S2D) using deepTools2 (Ramirez et al. 2016). To score the number of motifs, overlapping *sox* or *pou:sox* motifs were merged and trimmed to 20 bp. The numbers of non-redundant matches for *pou:sox* and *sox* per 320 bp genomic region was scored. See the results on Fig. 3G and Fig.4C.

RNA-seq, data processing and visualization.

The embryos were synchronized at the four cell stage and collected every 30 minutes starting from 2.5 hpf (pre-ZGA, 256 cell stage, 8th cell cycle) till midgastrula (6 hpf). 40-45 WT, MZ*spg*, MZ*sox19b* and MZ*sox19bspg* zebrafish embryos were collected, sorted and fixed in liquid nitrogen for each time point. Total RNA was isolated with QIAGEN RNeasy kit following the user's manual. We checked RNA quantity and quality by using Agilent RNA 6000 nano Kit on Agilent Bioanalyzer, according to manufacturer instructions. Poly-A enriched library preparation and single-end 50bp sequencing (35M reads per sample) on Illumina platform was performed by NOVOGENE company (China) for each sample. In total, we sequenced 78 samples in four biological replicates (Fig.5A) and 23 technical replicates for WT and single mutants (GEO: GSE137424). Further data processing was performed on european Galaxy server usegalaxy.eu (Afgan et al., 2016). All sequenced clean reads data were trimmed on 5' end for 5 bp by Trim Galore! program according to the sequencing quality control. Trimmed reads were mapped to danRer 11 using RNA STAR (Dobin et al., 2013) and ENSEMBL gene models. Number of reads for each gene was counted in Feature count program (Liao et al., 2014). Feature counts were cross-normalized using DEseq2 (Love et al., 2014). Processed RNA-seq data table deposited in GEO: GSE137424 was used for plotting expression profiles for single genes in Excel and as an input for RNA-sense. In our time series data, single 6 hpf data point was missing in one of the two biological replicates for MZ*sox19bspg* and in parallel WT control sample (Fig.5A). These missing 6 hpf time points for WT and MZ*sox19bspg* were duplicated from the other replicate to get an input for RNA-sense program. RNA-sense analysis was run with the following user-defined parameters (see sub-chapter "RNA-sense program" below for explanations): pVal switch=0.15, pVal FC=0.01, FC=2, threshold=100. To identify zygotic genes downregulated in the mutants (Fig.5C,D), Step 1 of RNA-sense was performed for the wild-type condition. To identify zygotic genes upregulated in the mutants at 5.5 hpf (Fig.6A-C), Step 1 of RNA-sense was performed for the mutant condition.

RNA-sense program

In order to facilitate the biological interpretation of time-resolved RNA-seq data, we developed a 3-step procedure called RNA-sense (see Fig. S6A, B). In principle, the usage of RNA-sense is not only restricted to RNA time series. RNA-sense can be applied to compare two groups of data series to capture the differences in the dynamic changes between the groups. The series data could be temporal, spatial, or any other continuous condition like series concentration of drug treatment. The data itself could be any sequencing data, including DNA, RNA and protein, or any other comparable large datasets.

In step one, time-resolved RNA-seq data in one of two conditions, e.g. the wild-type (user-defined parameter ExperimentStepDetection="WT"), are analyzed with respect to their temporal profile. The transcripts expressed below a user-defined threshold are excluded from the analysis. First, for each gene and for each measurement time point t, dynamic data is split into two groups before and after (after and equal to) time point t. The data is fitted by both a one-step model (two different means before and after time point t) and by a constant model (mean over all data points) and models are compared pairwise by means of likelihood ratio tests for each time point t. If the one-step model is significantly better (with user-defined p-value cutoff, pVal switch) than the constant model, a switch is detected for this time point. The difference of the means before and after the time point defines the direction of the switch "up" or "down". If switches were detected at different time points for each gene, the first possible time point is chosen.

In step two, fold changes between wild-type and mutant data are analyzed. For each gene and for each time point, Robinson and Smyth exact negative binomial test (with user-defined p-value cutoff, pVal FC) is performed to determine whether genes are significantly up- or downregulated in the mutant with respect to wild-type. The function exact.nb.test from the R package NBPSeq is used for analysis (https://cran.rstudio.com/web/).

In step three, results of step one and two are combined. Genes are grouped in a matrix form with respect to switch time (y-coordinate) and mutant fold change (x-coordinate). Genes for which fold change was detected at several time points appear several times in the matrix (Fig.S6A, B). For each tile of the matrix, Fisher's exact test for non-randomness is performed to analyze the correlation between the two

properties switch time and fold change detection. Tiles with a low p-value in the Fisher test show a high correlation between switch time and fold change. This can be interpreted as a high number of genes for which the switch point is shifted in time in the mutant condition.
RNA-sense is a flexible tool with several user-defined parameters:
-ExperimentStepDetection: tells which of two conditions (i.e. WT or mutant) should be used for switch detection in Step 1
-threshold – the transcript is included in the analysis, if the expression value in at least one data point reaches the threshold.
-pVal switch – p-value threshold for switch detection in Step 1
-FC – fold change value threshold (optional) for Step 2
-pVal FC – p-value threshold for fold change analysis at Step 2
The code and example files for automatically performing the 3-step procedure are available in the R-package RNAsense that was developed jointly with the paper and which is available on Bioconductor https://bioconductor.org/.

In-vitro nucleosome predictions and HNARs.

Nucleosome prediction program from Kaplan et al. 2009 was integrated into the Galaxy platform using the Galaxy tool SDK planemo (https://github.com/galaxyproject/planemo) and following the best practices for Galaxy tool development (http://galaxy-iuc-standards.readthedocs.io/en/latest/best_practices.html). The tool was uploaded into the european Galaxy ToolShed (ref. https://www.ncbi.nlm.nih.gov/pubmed/25001293) and is available at the Galaxy instance. The sequences around 24310 TF-binding and control genomic regions (Veil et al., 2019, Table S1) were extended to 10 kb to account for the edge effects, and *in-vitro* nucleosome prediction value was derived for every bp. For visualization, Nucleosome predictions were converted to BigWig files in DeepTools2 and used for plotting in Deeptools (Fig. 3B, S1H,I, Fig. S2A,C) or in the UCSC browser (Fig. 3F). The maximal and minimal nucleosome prediction values within 320 bp around TF-binding and control regions and their genomic positions were taken from in Table S1 (Veil et al., 2019). To orient the genomic regions aligned on [nucmax] along ascending nucleosome prediction values, we searched for the min. nucleosome prediction at +/- 160 bp around [nucmax]. If the min. prediction was downstream of [nucmax], we reversed the strand from + to -. The strand for oriented plots is listed in Table S1(Veil et al., 2019). To rank 24310 TF-binding and control regions to quartiles according to in-vitro predicted nucleosome occupancy, the average nucleosome prediction value within the region 0-+150 bp was taken (Fig. S2A).

Propeller Twist shape

Propeller twist values for aligned groups of genomic sequences (Fig.S2A, F,G) were calculated on TFBS shape server at http://rohslab.cmb.usc.edu/TFBSshape/ ((Yang et al., 2014)

QUANTIFICATION AND STATISTICAL ANALYSIS

The sequencing coverage between the samples was normalized as rkpm (reads per million reads per one kilobase). Normalized difference between the mutant and wild-type (ΔmutMNase) was calculated as Δmut=((rpkm(mut)-rpkm(wt))/(rkpm(mut)+rpkm(wt)). Average ΔmutMNase values per 320 bp around HNAR were taken. For H3K27ac ChIP-seq, normalized difference between the mutant and wild-type (Δmut K27ac) was calculated as ((log2(ChIP/input)mut-log2(ChIP/input)wt)/(log2(ChIP/input)mut+log2(ChIP/input)wt)). Average Δmut K27ac values per 1kb around HNAR were taken. Data were analyzed using JMP (SAS Institute 2012 version 10) using one-way ANOVA and linear regression (Table S1).

DATA AND SOFTWARE AVAILABILITY

Software

RNA-sense software developed during this study is available at
https://bioconductor.org/packages/release/bioc/html/RNAsense.html

Data Resources

The accession numbers for sequencing data reported in this study are GEO: GSE143306, GSE125945 and GSE137424.

Afgan, E., Baker, D., van den Beek, M., Blankenberg, D., Bouvier, D., Cech, M., Chilton, J., Clements, D., Coraor, N., Eberhard, C., *et al.* (2016). The Galaxy platform for accessible, reproducible and collaborative biomedical analyses: 2016 update. Nucleic Acids Res *44*, W3-W10.

Afek, A., Cohen, H., Barber-Zucker, S., Gordan, R., and Lukatsky, D.B. (2015). Nonconsensus Protein Binding to Repetitive DNA Sequence Elements Significantly Affects Eukaryotic Genomes. PLoS Comput Biol *11*, e1004429.

Almouzni, G., and Wolffe, A.P. (1995). Constraints on transcriptional activator function contribute to transcriptional quiescence during early Xenopus embryogenesis. The EMBO journal *14*, 1752-1765.

Amodeo, A.A., Jukam, D., Straight, A.F., and Skotheim, J.M. (2015). Histone titration against the genome sets the DNA-to-cytoplasm threshold for the Xenopus midblastula transition. Proc Natl Acad Sci U S A *112*, E1086-1095.

Avilion, A.A., Nicolis, S.K., Pevny, L.H., Perez, L., Vivian, N., and Lovell-Badge, R. (2003). Multipotent cell lineages in early mouse development depend on SOX2 function. Genes Dev *17*, 126-140.

Bachvarova, R., Davidson, E.H., Allfrey, V.G., and Mirsky, A.E. (1966). Activation of RNA synthesis associated with gastrulation. Proc Natl Acad Sci U S A *55*, 358-365.

Bogdanovic, O., Fernandez-Minan, A., Tena, J.J., de la Calle-Mustienes, E., Hidalgo, C., van Kruysbergen, I., van Heeringen, S.J., Veenstra, G.J., and Gomez-Skarmeta, J.L. (2012). Dynamics of enhancer chromatin signatures mark the transition from pluripotency to cell specification during embryogenesis. Genome Res *22*, 2043-2053.

Belting, H.G., Wendik, B., Lunde, K., Leichsenring, M., Mossner, R., Driever, W., and Onichtchouk, D. (2011). Pou5f1 contributes to dorsoventral patterning by positive regulation of vox and modulation of fgf8a expression. Dev biol *356(2):323-36*, 323-336.

Biddle, J.W., Nguyen, M., and Gunawardena, J. (2019). Negative reciprocity, not ordered assembly, underlies the interaction of Sox2 and Oct4 on DNA. Elife *8*.

Bischof, J., and Driever, W. (2004). Regulation of hhex expression in the yolk syncytial layer, the potential Nieuwkoop center homolog in zebrafish. Developmental biology *276*, 552-562.

Bogdanovic, O., Fernandez-Minan, A., Tena, J.J., de la Calle-Mustienes, E., Hidalgo, C., van Kruysbergen, I., van Heeringen, S.J., Veenstra, G.J., and Gomez-Skarmeta, J.L. (2012). Dynamics of enhancer chromatin signatures mark the transition from pluripotency to cell specification during embryogenesis. Genome Res *22*, 2043-2053.

Bowman, G.D., and Poirier, M.G. (2015). Post-translational modifications of histones that influence nucleosome dynamics. Chem Rev *115*, 2274-2295.

Boyer, L.A., Lee, T.I., Cole, M.F., Johnstone, S.E., Levine, S.S., Zucker, J.P., Guenther, M.G., Kumar, R.M., Murray, H.L., Jenner, R.G., *et al.* (2005). Core transcriptional regulatory circuitry in human embryonic stem cells. Cell *122*, 947-956.

Brown, J.L., Snir, M., Noushmehr, H., Kirby, M., Hong, S.K., Elkahloun, A.G., and Feldman, B. (2008). Transcriptional profiling of endogenous germ layer precursor cells identifies dusp4 as an essential gene in zebrafish endoderm specification. Proc Natl Acad Sci U S A *105*, 12337-12342.

Bruce, A.E., Howley, C., Zhou, Y., Vickers, S.L., Silver, L.M., King, M.L., and Ho, R.K. (2003). The maternally expressed zebrafish T-box gene eomesodermin regulates organizer formation. Development *130*, 5503-5517.

Cermak, T., Doyle, E.L., Christian, M., Wang, L., Zhang, Y., Schmidt, C., Baller, J.A., Somia, N.V., Bogdanove, A.J., and Voytas, D.F. (2011). Efficient design and assembly of custom TALEN and other TAL effector-based constructs for DNA targeting. Nucleic Acids Research *39*, e82.

Chan, S.H., Tang, Y., Miao, L., Darwich-Codore, H., Vejnar, C.E., Beaudoin, J.D., Musaev, D., Fernandez, J.P., Benitez, M.D.J., Bazzini, A.A., *et al.* (2019). Brd4 and P300 Confer Transcriptional Competency during Zygotic Genome Activation. Dev Cell *49*, 867-881 e868.
Charney, R.M., Forouzmand, E., Cho, J.S., Cheung, J., Paraiso, K.D., Yasuoka, Y., Takahashi, S., Taira, M., Blitz, I.L., Xie, X., *et al.* (2017). Foxh1 Occupies cis-Regulatory Modules Prior to Dynamic Transcription Factor Interactions Controlling the Mesendoderm Gene Program. Dev Cell *40*, 595-607 e594.
Chen, J., Zhang, Z., Li, L., Chen, B.C., Revyakin, A., Hajj, B., Legant, W., Dahan, M., Lionnet, T., Betzig, E., *et al.* (2014). Single-molecule dynamics of enhanceosome assembly in embryonic stem cells. Cell *156*, 1274-1285.
Chiu, T.P., Xin, B., Markarian, N., Wang, Y., and Rohs, R. (2019). TFBSshape: an expanded motif database for DNA shape features of transcription factor binding sites. Nucleic Acids Res.
Chronis, C., Fiziev, P., Papp, B., Butz, S., Bonora, G., Sabri, S., Ernst, J., and Plath, K. (2017). Cooperative Binding of Transcription Factors Orchestrates Reprogramming. Cell *168*, 442-459 e420.
Creyghton, M.P., Cheng, A.W., Welstead, G.G., Kooistra, T., Carey, B.W., Steine, E.J., Hanna, J., Lodato, M.A., Frampton, G.M., Sharp, P.A., *et al.* (2010). Histone H3K27ac separates active from poised enhancers and predicts developmental state. Proc Natl Acad Sci U S A *107*, 21931-21936.
Dal-Pra, S., Furthauer, M., Van-Celst, J., Thisse, B., and Thisse, C. (2006). Noggin1 and Follistatin-like2 function redundantly to Chordin to antagonize BMP activity. Developmental biology *298*, 514-526.
Dal-Pra, S., Thisse, C., and Thisse, B. (2011). FoxA transcription factors are essential for the development of dorsal axial structures. Dev Biol *350*, 484-495.
De Iaco, A., Planet, E., Coluccio, A., Verp, S., Duc, J., and Trono, D. (2017). DUX-family transcription factors regulate zygotic genome activation in placental mammals. Nat Genet *49*, 941-945.
De Robertis, E.M. (2009). Spemann's organizer and the self-regulation of embryonic fields. Mech Develop *126*, 925-941.
Dee, C.T., Gibson, A., Rengifo, A., Sun, S.K., Patient, R.K., and Scotting, P.J. (2007). A change in response to Bmp signalling precedes ectodermal fate choice. Int J Dev Biol *51*, 79-84.
Dobin, A., Davis, C.A., Schlesinger, F., Drenkow, J., Zaleski, C., Jha, S., Batut, P., Chaisson, M., and Gingeras, T.R. (2013). STAR: ultrafast universal RNA-seq aligner. Bioinformatics *29*, 15-21.
Dogan, N., Wu, W., Morrissey, C.S., Chen, K.B., Stonestrom, A., Long, M., Keller, C.A., Cheng, Y., Jain, D., Visel, A., *et al.* (2015). Occupancy by key transcription factors is a more accurate predictor of enhancer activity than histone modifications or chromatin accessibility. Epigenetics Chromatin *8*, 16.
Du, S., Draper, B.W., Mione, M., Moens, C.B., and Bruce, A. (2012). Differential regulation of epiboly initiation and progression by zebrafish Eomesodermin A. Developmental biology *362*, 11-23.
Dubrulle, J., Jordan, B.M., Akhmetova, L., Farrell, J.A., Kim, S.H., Solnica-Krezel, L., and Schier, A.F. (2015). Response to Nodal morphogen gradient is determined by the kinetics of target gene induction. eLife *4*.
Eckerle, S., Ringler, M., Lecaudey, V., Nitschke, R., and Driever, W. (2018). Progesterone modulates microtubule dynamics and epiboly progression during zebrafish gastrulation. Dev Biol *434*, 249-266.
Eckersley-Maslin, M., Alda-Catalinas, C., Blotenburg, M., Kreibich, E., Krueger, C., and Reik, W. (2019). Dppa2 and Dppa4 directly regulate the Dux-driven zygotic transcriptional program. Genes Dev *33*, 194-208.

Fekany, K., Yamanaka, Y., Leung, T., Sirotkin, H.I., Topczewski, J., Gates, M.A., Hibi, M., Renucci, A., Stemple, D., Radbill, A., *et al.* (1999). The zebrafish bozozok locus encodes Dharma, a homeodomain protein essential for induction of gastrula organizer and dorsoanterior embryonic structures. Development *126*, 1427-1438.

Feldman, B., Gates, M.A., Egan, E.S., Dougan, S.T., Rennebeck, G., Sirotkin, H.I., Schier, A.F., and Talbot, W.S. (1998). Zebrafish organizer development and germ-layer formation require nodal-related signals. Nature *395*, 181-185.

Feng, J., Liu, T., Qin, B., Zhang, Y., and Liu, X.S. (2012). Identifying ChIP-seq enrichment using MACS. Nat Protoc *7*, 1728-1740.

Ferg, M., Sanges, R., Gehrig, J., Kiss, J., Bauer, M., Lovas, A., Szabo, M., Yang, L., Straehle, U., Pankratz, M.J., *et al.* (2007). The TATA-binding protein regulates maternal mRNA degradation and differential zygotic transcription in zebrafish. EMBO J *26*, 3945-3956.

Friman, E.T., Deluz, C., Meireles-Filho, A.C., Govindan, S., Gardeux, V., Deplancke, B., and Suter, D.M. (2019). Dynamic regulation of chromatin accessibility by pluripotency transcription factors across the cell cycle. Elife *8*.

Frum, T., Halbisen, M.A., Wang, C., Amiri, H., Robson, P., and Ralston, A. (2013). Oct4 cell-autonomously promotes primitive endoderm development in the mouse blastocyst. Developmental cell *25*, 610-622.

Furthauer, M., Thisse, B., and Thisse, C. (1999). Three different noggin genes antagonize the activity of bone morphogenetic proteins in the zebrafish embryo. Developmental biology *214*, 181-196.

Gagnon, J.A., Obbad, K., and Schier, A.F. (2018). The primary role of zebrafish nanog is in extra-embryonic tissue. Development *145*.

Gao, L., Wu, K., Liu, Z., Yao, X., Yuan, S., Tao, W., Yi, L., Yu, G., Hou, Z., Fan, D., *et al.* (2018). Chromatin Accessibility Landscape in Human Early Embryos and Its Association with Evolution. Cell *173*, 248-259 e215.

Gentsch, G.E., Spruce, T., Owens, N.D.L., and Smith, J.C. (2019). The role of maternal pioneer factors in predefining first zygotic responses to inductive signals. bioRxiv, 306803.

Gerhart, J. (1980). Mechanisms regulating pattern formation in the amphibian egg and early embryo. In Biological Regulation and Development, R. Goldberg, ed. (New York: Plenum Press), pp. 133–315.

Giorgetti, A., Montserrat, N., Rodriguez-Piza, I., Azqueta, C., Veiga, A., and Izpisua Belmonte, J.C. (2010). Generation of induced pluripotent stem cells from human cord blood cells with only two factors: Oct4 and Sox2. Nat Protoc *5*, 811-820.

Haberle, V., Li, N., Hadzhiev, Y., Plessy, C., Previti, C., Nepal, C., Gehrig, J., Dong, X., Akalin, A., Suzuki, A.M., *et al.* (2014). Two independent transcription initiation codes overlap on vertebrate core promoters. Nature *507*, 381-385.

Harvey, S.A., Sealy, I., Kettleborough, R., Fenyes, F., White, R., Stemple, D., and Smith, J.C. (2013). Identification of the zebrafish maternal and paternal transcriptomes. Development *140*, 2703-2710.

Hiller, M., Agarwal, S., Notwell, J.H., Parikh, R., Guturu, H., Wenger, A.M., and Bejerano, G. (2013). Computational methods to detect conserved non-genic elements in phylogenetically isolated genomes: application to zebrafish. Nucleic Acids Res *41*, e151.

He, H.H., Meyer, C.A., Shin, H., Bailey, S.T., Wei, G., Wang, Q., Zhang, Y., Xu, K., Ni, M., Lupien, M., *et al.* (2010). Nucleosome dynamics define transcriptional enhancers. Nature genetics *42*, 343-347.

Heintzman, N.D., Stuart, R.K., Hon, G., Fu, Y., Ching, C.W., Hawkins, R.D., Barrera, L.O., Van Calcar, S., Qu, C., Ching, K.A., *et al.* (2007). Distinct and predictive chromatin signatures of transcriptional promoters and enhancers in the human genome. Nature genetics *39*, 311-318.

Hendrickson, P.G., Dorais, J.A., Grow, E.J., Whiddon, J.L., Lim, J.W., Wike, C.L., Weaver, B.D., Pflueger, C., Emery, B.R., Wilcox, A.L., *et al.* (2017). Conserved roles of mouse DUX

and human DUX4 in activating cleavage-stage genes and MERVL/HERVL retrotransposons. Nat Genet *49*, 925-934.
Hiller, M., Agarwal, S., Notwell, J.H., Parikh, R., Guturu, H., Wenger, A.M., and Bejerano, G. (2013). Computational methods to detect conserved non-genic elements in phylogenetically isolated genomes: application to zebrafish. Nucleic Acids Res *41*, e151.
Hong, S.K., Jang, M.K., Brown, J.L., McBride, A.A., and Feldman, B. (2011). Embryonic mesoderm and endoderm induction requires the actions of non-embryonic Nodal-related ligands and Mxtx2. Development *138*, 787-795.
Hou, L., Srivastava, Y., and Jauch, R. (2017). Molecular basis for the genome engagement by Sox proteins. Semin Cell Dev Biol *63*, 2-12.
Howe, K., Clark, M.D., Torroja, C.F., Torrance, J., Berthelot, C., Muffato, M., Collins, J.E., Humphray, S., McLaren, K., Matthews, L., *et al.* (2013). The zebrafish reference genome sequence and its relationship to the human genome. Nature *496*, 498-503.
Huangfu, D., Osafune, K., Maehr, R., Guo, W., Eijkelenboom, A., Chen, S., Muhlestein, W., and Melton, D.A. (2008). Induction of pluripotent stem cells from primary human fibroblasts with only Oct4 and Sox2. Nat Biotechnol *26*, 1269-1275.
Iwafuchi-Doi, M., and Zaret, K.S. (2016). Cell fate control by pioneer transcription factors. Development *143*, 1833-1837.
Joseph, S.R., Palfy, M., Hilbert, L., Kumar, M., Karschau, J., Zaburdaev, V., Shevchenko, A., and Vastenhouw, N.L. (2017). Competition between histone and transcription factor binding regulates the onset of transcription in zebrafish embryos. Elife *6*.
Kafiani, C.A., Timofeeva, M.J., Neyfakh, A.A., Melnikova, N.L., and Rachkus, J.A. (1969). RNA synthesis in te early embryogenesis of a fish (Misgurnus fossilis). J Embryol Exp Morphol *21*, 295-308.
Kane, D.A., and Kimmel, C.B. (1993). The zebrafish midblastula transition. Development *119*, 447-456.
Kaplan, N., Moore, I.K., Fondufe-Mittendorf, Y., Gossett, A.J., Tillo, D., Field, Y., LeProust, E.M., Hughes, T.R., Lieb, J.D., Widom, J., *et al.* (2009). The DNA-encoded nucleosome organization of a eukaryotic genome. Nature *458*, 362-366.
Kawahara, A., Wilm, T., Solnica-Krezel, L., and Dawid, I.B. (2000). Antagonistic role of vega1 and bozozok/dharma homeobox genes in organizer formation. Proc Natl Acad Sci U S A *97*, 12121-12126.
Keller, P.J., Schmidt, A.D., Wittbrodt, J., and Stelzer, E.H. (2008). Reconstruction of zebrafish early embryonic development by scanned light sheet microscopy. Science *322*, 1065-1069.
Kikuchi, Y., Agathon, A., Alexander, J., Thisse, C., Waldron, S., Yelon, D., Thisse, B., and Stainier, D.Y. (2001). casanova encodes a novel Sox-related protein necessary and sufficient for early endoderm formation in zebrafish. Genes Dev *15*, 1493-1505.
Kikuchi, Y., Trinh, L.A., Reiter, J.F., Alexander, J., Yelon, D., and Stainier, D.Y. (2000). The zebrafish bonnie and clyde gene encodes a Mix family homeodomain protein that regulates the generation of endodermal precursors. Genes Dev *14*, 1279-1289.
Kimmel, C.B., Ballard, W.W., Kimmel, S.R., Ullmann, B., and Schilling, T.F. (1995). Stages of embryonic development of the zebrafish. Dev Dyn *203*, 253-310.
Klemm, S.L., Shipony, Z., and Greenleaf, W.J. (2019). Chromatin accessibility and the regulatory epigenome. Nat Rev Genet *20*, 207-220.
Koos, D.S., and Ho, R.K. (1999). The nieuwkoid/dharma homeobox gene is essential for bmp2b repression in the zebrafish pregastrula. Dev Biol *215*, 190-207.
Kotkamp, K., Kur, E., Wendik, B., Polok, B.K., Ben-Dor, S., Onichtchouk, D., and Driever, W. (2014a). Pou5f1/Oct4 Promotes Cell Survival via Direct Activation of mych Expression during Zebrafish Gastrulation. PLoS One *9*, e92356.
Kotkamp, K., Mossner, R., Allen, A., Onichtchouk, D., and Driever, W. (2014b). A Pou5f1/Oct4 dependent Klf2a, Klf2b, and Klf17 regulatory sub-network contributes to EVL

and ectoderm development during zebrafish embryogenesis. Developmental biology *385*, 433-447.

Kuo, C.L., Lam, C.M., Hewitt, J.E., and Scotting, P.J. (2013). Formation of the embryonic organizer is restricted by the competitive influences of Fgf signaling and the SoxB1 transcription factors. PLoS One *8*, e57698.

Langmead, B., and Salzberg, S.L. (2012). Fast gapped-read alignment with Bowtie 2. Nat Methods *9*, 357-359.

Lee, M.T., Bonneau, A.R., Takacs, C.M., Bazzini, A.A., Divito, K.R., Fleming, E.S., and Giraldez, A.J. (2013). Nanog, Pou5f1 and SoxB1 activate zygotic gene expression during the maternal-to-zygotic transition. Nature, 360-364.

Leichsenring, M., Maes, J., Mossner, R., Driever, W., and Onichtchouk, D. (2013). Pou5f1 transcription factor controls zygotic gene activation in vertebrates. Science *341*, 1005-1009.

Leung, T., Bischof, J., Soll, I., Niessing, D., Zhang, D., Ma, J., Jackle, H., and Driever, W. (2003). bozozok directly represses bmp2b transcription and mediates the earliest dorsoventral asymmetry of bmp2b expression in zebrafish. Development *130*, 3639-3649.

Li, S., Zheng, E.B., Zhao, L., and Liu, S. (2019). Nonreciprocal and Conditional Cooperativity Directs the Pioneer Activity of Pluripotency Transcription Factors. Cell Rep *28*, 2689-2703 e2684.

Liang, H.L., Nien, C.Y., Liu, H.Y., Metzstein, M.M., Kirov, N., and Rushlow, C. (2008). The zinc-finger protein Zelda is a key activator of the early zygotic genome in Drosophila. Nature *456*, 400-403.

Liao, Y., Smyth, G.K., and Shi, W. (2014). featureCounts: an efficient general purpose program for assigning sequence reads to genomic features. Bioinformatics *30*, 923-930.

Liu, G., Wang, W., Hu, S., Wang, X., and Zhang, Y. (2018). Inherited DNA methylation primes the establishment of accessible chromatin during genome activation. Genome Res *28*, 998-1007.

Liu, Z., Ning, G., Xu, R., Cao, Y., Meng, A., and Wang, Q. (2016). Fscn1 is required for the trafficking of TGF-beta family type I receptors during endoderm formation. Nat Commun *7*, 12603.

Loh, Y.H., Wu, Q., Chew, J.L., Vega, V.B., Zhang, W., Chen, X., Bourque, G., George, J., Leong, B., Liu, J., *et al.* (2006). The Oct4 and Nanog transcription network regulates pluripotency in mouse embryonic stem cells. Nat Genet *38*, 431-440.

Love, M.I., Huber, W., and Anders, S. (2014). Moderated estimation of fold change and dispersion for RNA-seq data with DESeq2. Genome Biol *15*, 550.

Lu, F., Liu, Y., Inoue, A., Suzuki, T., Zhao, K., and Zhang, Y. (2016). Establishing Chromatin Regulatory Landscape during Mouse Preimplantation Development. Cell *165*, 1375-1388.

Lunde, K., Belting, H.G., and Driever, W. (2004). Zebrafish pou5f1/pou2, homolog of mammalian Oct4, functions in the endoderm specification cascade. Current biology : CB *14*, 48-55.

McDaniel, S.L., Gibson, T.J., Schulz, K.N., Fernandez Garcia, M., Nevil, M., Jain, S.U., Lewis, P.W., Zaret, K.S., and Harrison, M.M. (2019). Continued Activity of the Pioneer Factor Zelda Is Required to Drive Zygotic Genome Activation. Mol Cell *74*, 185-195 e184.

Melby, A.E., Beach, C., Mullins, M., and Kimelman, D. (2000). Patterning the early zebrafish by the opposing actions of bozozok and vox/vent. Dev Biol *224*, 275-285.

Montserrat, N., Ramirez-Bajo, M.J., Xia, Y., Sancho-Martinez, I., Moya-Rull, D., Miquel-Serra, L., Yang, S., Nivet, E., Cortina, C., Gonzalez, F., *et al.* (2012). Generation of induced pluripotent stem cells from human renal proximal tubular cells with only two transcription factors, OCT4 and SOX2. J Biol Chem *287*, 24131-24138.

Nelson, A.C., Cutty, S.J., Niini, M., Stemple, D.L., Flicek, P., Houart, C., Bruce, A.E., and Wardle, F.C. (2014). Global identification of Smad2 and Eomesodermin targets in zebrafish

identifies a conserved transcriptional network in mesendoderm and a novel role for Eomesodermin in repression of ectodermal gene expression. BMC Biol *12*, 81.
Newport, J., and Kirschner, M. (1982a). A major developmental transition in early Xenopus embryos: I. characterization and timing of cellular changes at the midblastula stage. Cell *30*, 675-686.
Newport, J., and Kirschner, M. (1982b). A major developmental transition in early Xenopus embryos: II. Control of the onset of transcription. Cell *30*, 687-696.
Neyfakh, A.A. (1959). X-ray inactivation of nuclei as method for studying their function in the early development of fishes. Journal of embryology and experimental morphology *7*, 173-192.
Neyfakh, A.A. (1964). Radiation Investigation of Nucleo-Cytoplasmic Interrelations in Morphogenesis and Biochemical Differentiation. Nature *201*, 880-884.
Okuda, Y., Ogura, E., Kondoh, H., and Kamachi, Y. (2010). B1 SOX coordinate cell specification with patterning and morphogenesis in the early zebrafish embryo. PLoS Genetics *6*, e1000936.
Okuda, Y., Yoda, H., Uchikawa, M., Furutani-Seiki, M., Takeda, H., Kondoh, H., and Kamachi, Y. (2006). Comparative genomic and expression analysis of group B1 sox genes in zebrafish indicates their diversification during vertebrate evolution. Developmental dynamics : an official publication of the American Association of Anatomists *235*, 811-825.
Onichtchouk, D., Geier, F., Polok, B., Messerschmidt, D.M., Mossner, R., Wendik, B., Song, S., Taylor, V., Timmer, J., and Driever, W. (2010). Zebrafish Pou5f1-dependent transcriptional networks in temporal control of early development. Mol Syst Biol *6*, 354.
Palfy, M., Schulze, G., Valen, E., and Vastenhouw, N.L. (2020). Chromatin accessibility established by Pou5f3, Sox19b and Nanog primes genes for activity during zebrafish genome activation. PLoS Genet *16*, e1008546.
Paraiso, K.D., Blitz, I.L., Coley, M., Cheung, J., Sudou, N., Taira, M., and Cho, K.W.Y. (2019). Endodermal Maternal Transcription Factors Establish Super-Enhancers during Zygotic Genome Activation. Cell Rep *27*, 2962-2977 e2965.
Poulain, M., and Lepage, T. (2002). Mezzo, a paired-like homeobox protein is an immediate target of Nodal signalling and regulates endoderm specification in zebrafish. Development *129*, 4901-4914.
Quinlan, A.R., and Hall, I.M. (2010). BEDTools: a flexible suite of utilities for comparing genomic features. Bioinformatics *26*, 841-842.
Ramel, M.C., and Lekven, A.C. (2004). Repression of the vertebrate organizer by Wnt8 is mediated by Vent and Vox. Development *131*, 3991-4000.
Ramirez, F., Ryan, D.P., Gruning, B., Bhardwaj, V., Kilpert, F., Richter, A.S., Heyne, S., Dundar, F., and Manke, T. (2016). deepTools2: a next generation web server for deep-sequencing data analysis. Nucleic Acids Res *44*, W160-165.
Reid, C.D., Zhang, Y., Sheets, M.D., and Kessler, D.S. (2012). Transcriptional integration of Wnt and Nodal pathways in establishment of the Spemann organizer. Dev Biol *368*, 231-241.
Reim, G., and Brand, M. (2006). Maternal control of vertebrate dorsoventral axis formation and epiboly by the POU domain protein Spg/Pou2/Oct4. Development *133*, 2757-2770.
Reim, G., Mizoguchi, T., Stainier, D.Y., Kikuchi, Y., and Brand, M. (2004). The POU domain protein spg (pou2/Oct4) is essential for endoderm formation in cooperation with the HMG domain protein casanova. Dev Cell *6*, 91-101.
Reisser, M., Palmer, A., Popp, A.P., Jahn, C., Weidinger, G., and Gebhardt, J.C.M. (2018). Single-molecule imaging correlates decreasing nuclear volume with increasing TF-chromatin associations during zebrafish development. Nat Commun *9*, 5218.
Remenyi, A., Lins, K., Nissen, L.J., Reinbold, R., Scholer, H.R., and Wilmanns, M. (2003). Crystal structure of a POU/HMG/DNA ternary complex suggests differential assembly of Oct4 and Sox2 on two enhancers. Genes Dev *17*, 2048-2059.

Ruzicka, L., Howe, D.G., Ramachandran, S., Toro, S., Van Slyke, C.E., Bradford, Y.M., Eagle, A., Fashena, D., Frazer, K., Kalita, P., *et al.* (2019). The Zebrafish Information Network: new support for non-coding genes, richer Gene Ontology annotations and the Alliance of Genome Resources. Nucleic Acids Res *47*, D867-D873.

Samee, M.A.H., Bruneau, B.G., and Pollard, K.S. (2019). A De Novo Shape Motif Discovery Algorithm Reveals Preferences of Transcription Factors for DNA Shape Beyond Sequence Motifs. Cell Syst *8*, 27-42 e26.

Sato, Y., Hilbert, L., Oda, H., Wan, Y., Heddleston, J.M., Chew, T.L., Zaburdaev, V., Keller, P., Lionnet, T., Vastenhouw, N., *et al.* (2019). Histone H3K27 acetylation precedes active transcription during zebrafish zygotic genome activation as revealed by live-cell analysis. Development *146*.

Schulte-Merker, S., Lee, K.J., McMahon, A.P., and Hammerschmidt, M. (1997). The zebrafish organizer requires chordino. Nature *387*, 862-863.

Schulte-Merker, S., van Eeden, F.J., Halpern, M.E., Kimmel, C.B., and Nusslein-Volhard, C. (1994). no tail (ntl) is the zebrafish homologue of the mouse T (Brachyury) gene. Development *120*, 1009-1015.

Schulz, K.N., Bondra, E.R., Moshe, A., Villalta, J.E., Lieb, J.D., Kaplan, T., McKay, D.J., and Harrison, M.M. (2015). Zelda is differentially required for chromatin accessibility, transcription factor binding, and gene expression in the early Drosophila embryo. Genome Res *25*, 1715-1726.

Schulz, K.N., and Harrison, M.M. (2018). Mechanisms regulating zygotic genome activation. Nature Reviews Genetics.

Shih, Y.H., Kuo, C.L., Hirst, C.S., Dee, C.T., Liu, Y.R., Laghari, Z.A., and Scotting, P.J. (2010). SoxB1 transcription factors restrict organizer gene expression by repressing multiple events downstream of Wnt signalling. Development *137*, 2671-2681.

Shimizu, T., Yamanaka, Y., Nojima, H., Yabe, T., Hibi, M., and Hirano, T. (2002). A novel repressor-type homeobox gene, ved, is involved in dharma/bozozok-mediated dorsal organizer formation in zebrafish. Mech Dev *118*, 125-138.

Shimizu, T., Yamanaka, Y., Ryu, S.L., Hashimoto, H., Yabe, T., Hirata, T., Bae, Y.K., Hibi, M., and Hirano, T. (2000). Cooperative roles of Bozozok/Dharma and Nodal-related proteins in the formation of the dorsal organizer in zebrafish. Mech Dev *91*, 293-303.

Shindo, Y., and Amodeo, A.A. (2019). Dynamics of Free and Chromatin-Bound Histone H3 during Early Embryogenesis. Curr Biol *29*, 359-366 e354.

Signoret, J., and Lefresne, J. (1971). Contribution a L'etude de la segmentation de l'oeuf d'axolotl: I. Definition de la transition blastuleenne. Ann Embryol Morphog *4*, 113-123.

Sirotkin, H.I., Dougan, S.T., Schier, A.F., and Talbot, W.S. (2000). bozozok and squint act in parallel to specify dorsal mesoderm and anterior neuroectoderm in zebrafish. Development *127*, 2583-2592.

Slagle, C.E., Aoki, T., and Burdine, R.D. (2011). Nodal-dependent mesendoderm specification requires the combinatorial activities of FoxH1 and Eomesodermin. PLoS Genet *7*, e1002072.

Song, S., Eckerle, S., Onichtchouk, D., Marrs, J.A., Nitschke, R., and Driever, W. (2013). Pou5f1-dependent EGF expression controls E-cadherin endocytosis, cell adhesion, and zebrafish epiboly movements. Developmental cell *24*, 486-501.

Soufi, A., Garcia, M.F., Jaroszewicz, A., Osman, N., Pellegrini, M., and Zaret, K.S. (2015). Pioneer transcription factors target partial DNA motifs on nucleosomes to initiate reprogramming. Cell *161*, 555-568.

Sun, Y., Nien, C.Y., Chen, K., Liu, H.Y., Johnston, J., Zeitlinger, J., and Rushlow, C. (2015). Zelda overcomes the high intrinsic nucleosome barrier at enhancers during Drosophila zygotic genome activation. Genome Res, 1703–1714.

Takahashi, K., and Yamanaka, S. (2006). Induction of pluripotent stem cells from mouse embryonic and adult fibroblast cultures by defined factors. Cell *126*, 663-676. Epub 2006 Aug 2010.

Talbot, W.S., Trevarrow, B., Halpern, M.E., Melby, A.E., Farr, G., Postlethwait, J.H., Jowett, T., Kimmel, C.B., and Kimelman, D. (1995). A homeobox gene essential for zebrafish notochord development. Nature *378*, 150-157.

Tosic, J., Kim, G.J., Pavlovic, M., Schroder, C.M., Mersiowsky, S.L., Barg, M., Hofherr, A., Probst, S., Kottgen, M., Hein, L., *et al.* (2019). Eomes and Brachyury control pluripotency exit and germ-layer segregation by changing the chromatin state. Nat Cell Biol *21*, 1518-1531.

Varga, M., Maegawa, S., Bellipanni, G., and Weinberg, E.S. (2007). Chordin expression, mediated by Nodal and FGF signaling, is restricted by redundant function of two beta-catenins in the zebrafish embryo. Mech Dev *124*, 775-791. Epub 2007 Jun 2012.

Vastenhouw, N.L., Cao, W.X., and Lipshitz, H.D. (2019). The maternal-to-zygotic transition revisited. Development *146*.

Veenstra, G.J., Destree, O.H., and Wolffe, A.P. (1999). Translation of maternal TATA-binding protein mRNA potentiates basal but not activated transcription in Xenopus embryos at the midblastula transition. Mol Cell Biol *19*, 7972-7982.

Veil, M., Schaechtle, M.A., Gao, M., Kirner, V., Buryanova, L., Grethen, R., and Onichtchouk, D. (2018). Maternal Nanog is required for zebrafish embryo architecture and for cell viability during gastrulation. Development *145*.

Veil, M., Yampolsky, L., Gruening, B., and Onichtchouk, D. (2019). Pou5f3, SoxB1, and Nanog remodel chromatin on High Nucleosome Affinity Regions at Zygotic Genome Activation. Genome Res.

Voss, T.C., Schiltz, R.L., Sung, M.H., Yen, P.M., Stamatoyannopoulos, J.A., Biddie, S.C., Johnson, T.A., Miranda, T.B., John, S., and Hager, G.L. (2011). Dynamic exchange at regulatory elements during chromatin remodeling underlies assisted loading mechanism. Cell *146*, 544-554.

Westerfield, M. (2000). The zebrafish book. A guide for the laboratory use of zebrafish (Danio rerio). 4th ed edn (Univ. of Oregon Press, Eugene.).

Wicklow, E., Blij, S., Frum, T., Hirate, Y., Lang, R.A., Sasaki, H., and Ralston, A. (2014). HIPPO pathway members restrict SOX2 to the inner cell mass where it promotes ICM fates in the mouse blastocyst. PLoS Genet *10*, e1004618.

Wilky, H., Chari, S., Govindan, J., and Amodeo, A.A. (2019). Histone concentration regulates the cell cycle and transcription in early development. Development.

Wu, G., Han, D., Gong, Y., Sebastiano, V., Gentile, L., Singhal, N., Adachi, K., Fischedick, G., Ortmeier, C., Sinn, M., *et al.* (2013). Establishment of totipotency does not depend on Oct4A. Nature cell biology.

Xu, C., Fan, Z.P., Muller, P., Fogley, R., Dibiase, A., Trompouki, E., Unternaehrer, J., Xiong, F., Torregroza, I., Evans, T., *et al.* (2012). Nanog-like Regulates Endoderm Formation through the Mxtx2-Nodal Pathway. Developmental cell *22*, 625-638.

Yamanaka, Y., Mizuno, T., Sasai, Y., Kishi, M., Takeda, H., Kim, C.H., Hibi, M., and Hirano, T. (1998). A novel homeobox gene, dharma, can induce the organizer in a non-cell-autonomous manner. Genes Dev *12*, 2345-2353.

Yang, L., Zhou, T., Dror, I., Mathelier, A., Wasserman, W.W., Gordan, R., and Rohs, R. (2014). TFBSshape: a motif database for DNA shape features of transcription factor binding sites. Nucleic Acids Res *42*, D148-155.

Zhang, C., and Klymkowsky, M.W. (2007). The Sox axis, Nodal signaling, and germ layer specification. Differentiation; research in biological diversity *75*, 536-545.

Zhu, F., Farnung, L., Kaasinen, E., Sahu, B., Yin, Y., Wei, B., Dodonova, S.O., Nitta, K.R., Morgunova, E., Taipale, M., *et al.* (2018). The interaction landscape between transcription factors and the nucleosome. Nature *562*, 76-81.